University of South Alabama
JagWorks@USA

Theses and Dissertations | Graduate School

12-2023

Initiation Criteria for the Onset of Geomagnetic Substorms Based on Auroral Observations and Electrojet Current Signatures

Mayowa Michael Kayode-Adeoye

Follow this and additional works at: https://jagworks.southalabama.edu/theses_diss

 Part of the Atmospheric Sciences Commons, Electrical and Computer Engineering Commons, Engineering Science and Materials Commons, Geotechnical Engineering Commons, Other Engineering Commons, and the Physical Processes Commons

THE UNIVERSITY OF SOUTH ALABAMA
COLLEGE OF ENGINEERING

INITIATION CRITERIA FOR THE ONSET OF GEOMAGNETIC SUBSTORMS BASED ON AURORAL OBSERVATIONS AND ELECTROJET CURRENT SIGNATURES

BY

Mayowa Michael Kayode-Adeoye

A Thesis

Submitted to the Graduate Faculty of the University of South Alabama
in partial fulfillment of the requirements for the degree of

Master of Science
in
Electrical Engineering
December 2023

Approved: Edmund Spencer Date: 11/02/2023

Chair of Thesis Committee: Dr. Edmund Spencer

Nov 2, 2023

Committee Member: Dr. Saeed Latif

Nov 2, 2023

Committee Member: Dr. Eric Steward

Purbi Adhya Nov 2, 2023

Committee Member: Dr. Purbi Adhya

Hulya Kirkici Nov 3, 2023

Chair of Department: Dr. Hulya Kirkici

Nov 16, 2023

Director of Graduate Studies: Dr. Clive Woods

Nov 27, 2023

Dean of the Graduate School: Dr. J. Harold Pardue

INITIATION CRITERIA FOR THE ONSET OF GEOMAGNETIC SUBSTORMS BASED ON AURORAL OBSERVATIONS AND ELECTROJET CURRENT SIGNATURES

A Thesis

Submitted to the Graduate Faculty of the
University of South Alabama
in partial fulfillment of the
requirements for the degree of

Master of Science

in

Electrical Engineering

by

Mayowa Michael Kayode-Adeoye
B.S., University of Lagos, 2018
December 2023

ACKNOWLEDGEMENTS

I would like to thank and express my gratitude to my advisor Dr. Edmund Spencer who continuously supported me throughout this research. Without his valuable feedback and knowledge in the field of Space Science and Electromagnetism, it would be impossible for me to achieve the goals of this research. I would like to thank Dr. Hulya Kirkici, Chair of the ECE department, for her continuous support. I am also indebted to all the faculty members and staff members of the ECE department for their help and support. I am grateful to my parents, friends, and family who always motivated me to achieve my academic goals and provided the necessary support. Lastly, I want to thank my friends and colleagues at the University of South Alabama for helping me on numerous occasions. Also, a big thanks go to Dr. Purbi Adhya for her substantial contributions.

TABLE OF CONTENTS

Page

LIST OF TABLES

LIST OF FIGURES

LIST OF ABBREVIATIONS

AE	Auroral Electrojet
AURORA	Auroral Oval Radar Integration Analysis
CME	Coronal Mass Ejection
GEO	Geostationary Earth Orbit
GMD	Geomagnetic Disturbance
IMF	Interplanetary Magnetic Field
Kp	Planetary K-index (a measure of geomagnetic activity)
LEO	Low Earth Orbit (used for satellites)
MHD	Magnetohydrodynamics
MMS	Magnetospheric Multiscale Mission
PBI	Poleward Boundary Intensification
SEP	Solar Energetic Particle
SML	Super Magnetometer Local Index
SWx	Space Weather
THEMIS	Time History of Events and Macroscale Interactions during Substorms
UHF	Ultra-High Frequency
VHF	Very High Frequency

ABSTRACT

Mayowa Michael Kayode-Adeoye, M. S., University of South Alabama, December 2023 Initiation Criteria for the Onset of Geomagnetic Substorms Based on Auroral Observations and Electrojet Current Signatures. Chair of Committee. Edmund Spencer, Ph.D.

In recent years, several substorm onset criteria have been developed, either from auroral observations (many authors) or from auroral electrojet properties such as those described by (Forsyth et al., 2015; Maimaiti et al., 2019; Newell & Gjerloev, 2011; Partamies et al., 2011) The different criteria are being investigated using a low order physics model of the magnetosphere called WINDMI (Spencer et al., 2009) and inferences are being made in line with the WINDMI model. The model variables will be compared with the criteria for substorm onset proposed by examining the SML index

The WINDMI model uses solar wind and IMF measurements from ACE spacecraft as input to a system of 8 non-linear ordinary differential equations. The state variables of the differential equations represent the energy stored in the geomagnetic tail, central plasma sheet, ring current, and field-aligned currents. In this work, the relationship between the output of the WINDMI model and SML (True data) will be established for different events and the timing of the onset for each event, the model parameters, and the model intermediate state space variables are examined and analyzed.

CHAPTER I

INTRODUCTION

The concept of substorms was first introduced in the 1960s (Akasofu, 2004) to describe a sudden release of stored energy in the magnetosphere, resulting in dynamic changes in the magnetospheric and ionospheric systems. Substorms have been found to significantly alter the auroras in the polar region, as well as the magnetospheric magnetic field and plasma environments. Advancements in satellite observations, ground-based measurements, and computer simulations have provided valuable insights into the underlying processes of substorm onset. Satellites such as THEMIS (Time History of Events and Macroscale Interactions during Substorm) mission and the Magnetospheric Multiscale (MMS) mission have contributed significantly to our understanding of detailed measurements of magnetic field variations, particle populations, and plasma dynamics.

The goal of this research is to analytically evaluate the substorm onset criteria based on auroral observations and electrojet indices criteria and establish the relationship between ground-based magnetic indices and field-aligned currents. Furthermore, the analysis of the substorm events on March 09, 2008, and other recognized days will be evaluated and compared with the output from the WINDMI model. The chosen dates are significant dates for substorms because all of THEMIS (Time History of Events and

Macroscale Interactions during Substorms) deployed five satellites to study the substorm phenomenon and were able to show activities. The plasma physics-based WINDMI model uses the solar wind dynamo voltage, Vsw, generated by a particular solar wind-magnetosphere coupling function to drive eight ordinary differential equations describing the transfer of power through the geomagnetic tail, the ionosphere, and the ring current. The WINDMI model is derived by assuming a magnetospheric configuration.

1.1 Motivation

The earth's magnetic field, which shields the planet from solar radiation, has grown weaker due to an increase in substorm events. Understanding the factors that cause these occurrences and comprehending the variables that trigger these events has never been more crucial. The primary objective of this project is to compare onsets of different established models and employ a linear model to discern and comprehend the disparities among various substorm onset criteria.

Substorm onsets are marked by rapid changes in the dynamics of the magnetosphere, particle acceleration, and auroral intensification. These events have a substantial impact on satellite operations, space weather forecasting, and our overall understanding of magnetospheric processes. The key motivation for this research lies in the consistency of disparities between different models predicting substorm onset.

While there are diverse criteria for defining and identifying substorm onsets, many of them converge on comparable results and this convergence indicates that various methods can effectively capture the fundamental aspects of substorm onsets. It also

underscores the complexity and multifaceted nature of substorms, which can be observed and analyzed from various perspectives.

Different substorm onset criteria are frequently developed in response to advances in observational methods and theoretical knowledge. As scientists gain deeper insights into the underlying physical processes involved in substorm initiation, they continually update and enhance these criteria. The goal is to enhance our understanding of substorms and their impacts on the magnetosphere and the nearby space environment.

This research is motivated by several key considerations.

1. Addressing the disparities in substorm onset predictions from different techniques is a central focus of this research.
2. This work aims to achieve a comprehensive understanding of the criteria for substorm onsets by employing the WINDMI model. How these criteria influence observed substorm onset patterns and how they evolve with variations in key parameters such as inductance (L) and capacitance (C) which are synonymous with magnetotail current, and Inertia respectively will be investigated. This investigation encompasses the study of the behavior and interrelationships of critical variables like I1, dI1/dt, and dSML/dt.
3. Another critical aspect of this research is the exploration of the reasons behind the intersection of substorm onset times derived from various models when compared with the WINDMI model, particularly when L and C values deviate from nominal values by 5%, 10%, and 20%.
4. How Variations in L and C, specifically deviations of 5%, 10%, and 20%, impact the clustering tendencies of substorm onset counts will be studied. These findings are

instrumental in enhancing space weather forecasting, optimizing satellite operations, and deepening our overall comprehension of magnetospheric processes.

5. The ultimate objective of this research is to advance our understanding of substorms, their onset criteria, and their effects on the magnetosphere and the nearby space environment. This endeavor contributes significantly to improving space weather predictions and ensuring the reliable operation of satellites. Furthermore, it plays a pivotal role in unraveling the underlying physical processes responsible for substorm initiation.

1.2 Contributions and Lessons Learned

This thesis contributes to the field by proposing an enhanced predictive model for substorm activity incorporating the identified initiation criteria for more accurate forecasts. Modeling the substorm onset situation using IMF measurements from the ACE spacecraft as input into a system of 8 nonlinear ordinary differential equations where the state variables of the differential equations represent the energy stored in the geomagnetic tail, the central plasma sheet, ring current, and field-aligned currents. The output from the model is the current (I1) which compares with the real-time measure of geomagnetic activities and disturbances (SML).

WINDMI model is forced to stay consistent with satellite electric and magnetic field observations which makes tracking the magnetotail energy dynamics, field-aligned current contributions, and energy injections into the ring current possible and within allowable limits. The low order models are computationally less intensive and easier to visualize and interpret. During strong geomagnetic activity, the MHD simulations are more difficult to control because of the strongly nonlinear response of the

magnetosphere-ionosphere system. MHD models also do not describe processes in the inner magnetosphere such as the formation of the ring current.

To complement the MHD, fluid, and kinetic models, it is important to have low-dimensional models that attempt to analyze the global or overall behavior of the magnetosphere-ionosphere system by reducing or combining the dynamics of various sections to simulate the interaction between key energy components while being fast and computationally inexpensive.

In the plasma physics-based WINDMI model, the solar wind-magnetosphere coupling function drives eight ordinary differential equations that describe the power transmission through the geomagnetic tail, the ionosphere, and the ring current. The solar wind dynamo voltage (Vsw) is the most fundamental coupling function.

1.3 Organization of the Thesis

This thesis is comprised of six chapters. In the first chapter, the problem statement, research motivation, and contribution of this research are discussed. Chapter II goes through the background study of the challenges associated with Substorm Onset determination and the criteria of the models that are used.

A brief introduction to the model and equations is also presented in Chapter III contains the performance analysis of the different criteria for different events. Chapter IV contains the performance evaluation of the WINDMI model with varying input conditions on the studied events in Chapter III. In Chapter V, comparisons of the outputs of the studied events are discussed and a conclusion is established. Chapter VI discusses the future scope of the work of the thesis.

CHAPTER II

GEOMAGNETIC SUBSTORMS AND SUBSTORM ONSET

2.1 Introduction

A crucial mechanism for the transfer, storage, and release of energy in the solar wind-magnetosphere interaction is the Geomagnetic Substorm. Typically, it consists of several events, including aurora brightness, geomagnetic disturbances in various places, such as the polar regions, disruptions to the magnetotail current sheet, and injections of energetic particles (Fu et al., 2021; Kamide & Akasofu, 1975; Liu et al., 2007). The concept of substorms was first introduced in the 1960s (Akasofu, 2004) to describe a sudden release of stored energy in the magnetosphere, resulting in dynamic changes in the magnetospheric and ionospheric systems. Substorms have been found to significantly alter the auroras in the polar region, as well as the magnetospheric magnetic field and plasma environments.

There are three distinct phases to a geomagnetic substorm. Growth, Expansion, and Recovery phases. Enhanced magnetospheric convection allows solar wind energy to enter the magnetosphere during the growth phase, where it is stored in the magnetotail (Nishimura et al., 2016).

The aurora is produced by the disruption of the tail current sheet, the formation of the field-aligned current, and the precipitation of injected particles into the polar ionosphere during the expansion phase. The aurora and other disruptions weaken and eventually return to the quiet period condition during the recovery phase. Substorm frequency varies with the season, and prior research (Fu et al., 2021) offers several causes.

Substorm onset is an important process in the study of space weather and the dynamics of the Earth's magnetosphere. Changes in the solar wind and their subsequent interactions with the earth's magnetic field are the major cause of substorm. Substorms are powerful, dynamic phenomena that take place in the magnetosphere. Understanding the intricate mechanisms involved in substorm onset is crucial for comprehending the complex dynamics involved in this topic.

The classical model of substorm onset, known as the 'Substorm Growth Phase', involves several key stages.

1. The growth phase begins with the accumulation of magnetic energy in the magnetotail, a region of the magnetosphere that extends away from the Earth on the night side.
2. As the magnetic energy continues to build up, the magnetotail becomes stretched and elongated, storing energy in the form of a stretched and twisted magnetic field configuration.
3. At a critical threshold, the stored magnetic energy is rapidly released, initiating a substorm. This release is often associated with a process called 'Magnetic Reconnection.' Magnetic energy is converted into kinetic energy, thermal energy, and particle acceleration during reconnection (Mozer & Pritchett, 2010).

Substorm onset is accompanied by various dynamic phenomena, such as the expansion and intensification of the auroras, the formation of plasmoids (plasma flow channels), and the generation of energetic particles. Substorm onset is followed by the expansion phase, it is at this phase that the released energy propagates through the magnetosphere, causing changes in the magnetic field configuration and plasma dynamics. Despite significant progress, substorm onset remains an active area of research, as the exact mechanisms triggering the release of stored magnetic energy and the associated energy transfer processes are still not fully understood. Ongoing studies continue to refine existing models and explore new theories to enhance our understanding of the background and dynamics of substorm onset, improving our ability to predict and mitigate the impacts of space weather on technological systems and satellite communication.

2.2 Storms and Substorms

From the early days, it has been widely accepted that intense geomagnetic storms are correlated with spectacular auroral displays. However, back then both issues were handled nearly independently. Thus, it is interesting and intriguing to examine the history of research on the interaction between geomagnetic storms and auroral substorms. Understanding the formation of ring current is an interesting concept when it comes to storms and substorms as auroral storms are responsible for the main phase of geomagnetic substorms by injecting protons into the ring current belt (DeForest & McIlwain, 1971).

Geomagnetic Storms and Substorms are extreme events that are a part of what is known as Space Weather. These storms and substorms adversely affect satellite

communication equipment in space, large electrical power distribution grids, petroleum pipeline networks, and communication equipment on the ground by inducing electric and magnetic fields in the conductors.

Fluctuations in the earth's magnetic field during substorms can cause disruptions in the ionosphere, resulting in ionospheric scintillation. This scintillation leads to rapid fluctuations in signal amplitude, phase, and arrival angle, causing signal fading, increased noise, and errors in satellite communication. Solar energetic particles whose energies and densities are enhanced during storms cause operational problems for spacecraft and satellites by affecting the sensitive electronic equipment onboard.

The substorm is a fundamental geomagnetic process in the Earth's magnetosphere that has been a topic of intense research over several decades. Of particular interest is how the ionosphere, inner magnetosphere, and geotail dynamics influence the growth, onset, expansion, and recovery phases of a typical substorm (Juusola et al., 2011; Liu et al., 2007). These components may interact differently under varying solar wind conditions or different classes of sub-storm activity. Currently, there are three accepted classes of sub-storms. isolated sub-storms, storm time sub-storms, and Sawtooth events also known as periodic sub-storms (Partamies et al., 2011).

The analysis and prediction of geomagnetic substorms is an active effort at present. Satellites have been launched into space to obtain and process plasma data in front of the Earth's bow shock, in the magnetopause, the magnetotail, and the lobe cavity. In addition, ground-based monitoring stations are in strategic places throughout the world that carefully measure changes in the Earth's magnetic field and other geophysical quantities. These stations measurements are coordinated and combined appropriately to produce

geomagnetic indices including the Auroral Electrojet indices, the upper and lower auroral indices AU, AL, and the Dst (Storm Time Disturbance) index. Numerous other ground-based electromagnetic data from radars and optical instruments are collected to determine the state of the Earth's space environment.

2.3 Solar Wind Interaction with the Earth

The near-Earth space environment is significantly shaped by the interaction between the solar wind and the Earth's magnetosphere. The solar wind is a stream of charged particles, protons, and electrons constantly emanating from the sun. The sun emits a continuous stream of charged particles that flows outward into the interplanetary space called the Solar Wind. This solar wind is a magnetized plasma that is primarily composed of protons (about 90-95%) and electrons (about 5-10%). However, it also contains small amounts of heavier ions, such as helium, oxygen, carbon, etc. The interaction between the solar wind and the magnetosphere is shown below.

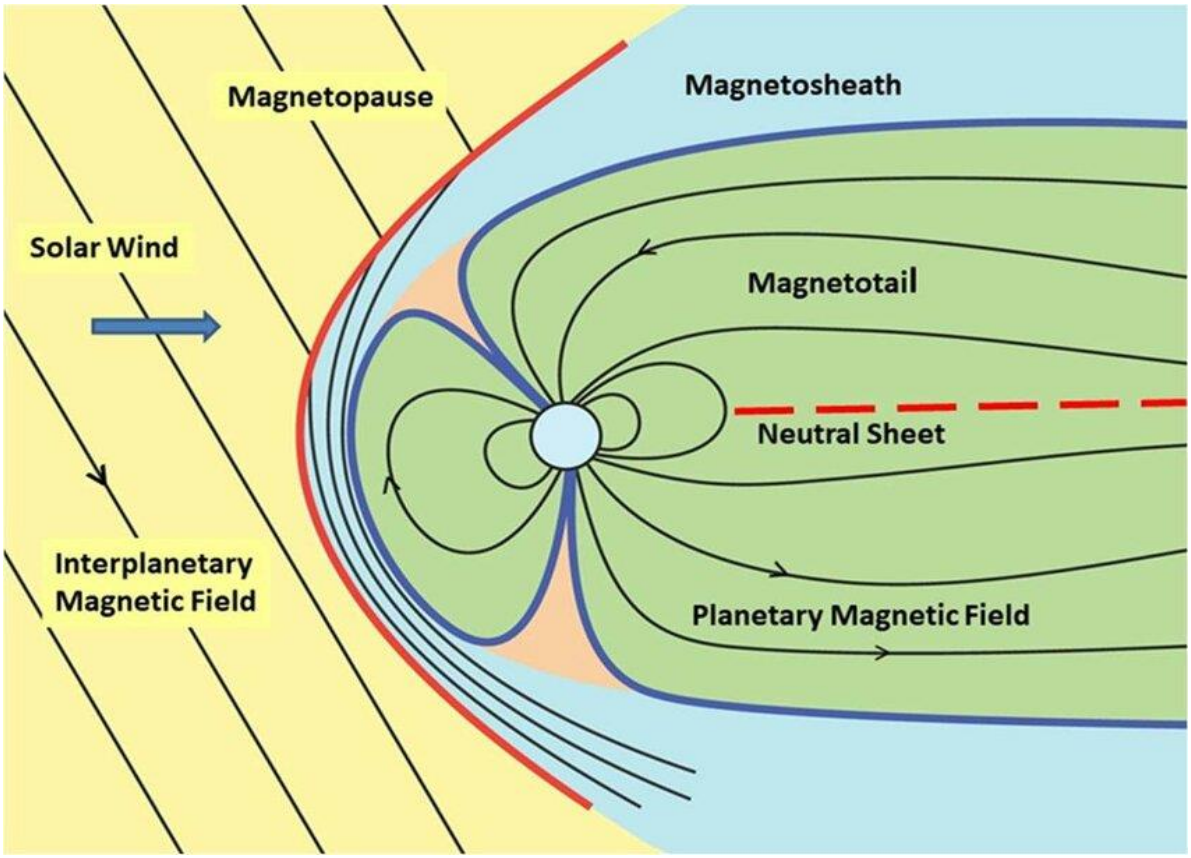

Figure 1. Illustration of the interaction between the solar wind and Earth's magnetosphere

In Figure 1, the red curved line delineates the bow shock, while the blue region represents the magnetosheath where magnetic fields (depicted as black lines) are draped and convected downstream. The magnetosphere and magnetotail are highlighted in green (Tsurutani et al., 2023).

According to NOAA (National Oceanic and Atmospheric Association), the speed of solar wind varies widely ranging from 300km/s to 800km/s but this changes during more active periods of the sun, where the speed can significantly increase, reaching several thousand km/s. The density of the solar wind is relatively low compared to the

density of the earth's atmosphere and it ranges between 5-10cm^3. The solar wind carries the Sun's magnetic field, which is embedded in plasma. The magnetic field lines in the solar wind can be highly variable and exhibit complex structures. These magnetic fields play a crucial role in the interaction between the solar wind and the Earth's magnetic field.

The magnetosphere formed by the interaction of the solar wind with the earth's magnetic field is a complex, dynamical structure with numerous energy reservoirs and transitional layers that separate the nightside geomagnetic lobes, central plasma sheet, and inner magnetospheric ring current. The solar wind electric field in the earth's reference frame drives substantial power through these components, a large fraction of which is dissipated in the ionosphere and the ring current through charge exchange collisions with neutral atoms. The transient power into the magnetosphere reaches levels up to 10^{12} W for periods of up to a day during storm times.

The Earth's magnetosphere is shown in the figure below. The bow shock separates the high-speed, low-density plasma in the solar wind from the low-speed, high-density, and high-temperature plasma in the magnetosheath. Magnetopause is a boundary layer that separates the plasmas of mixed solar and terrestrial origin from the magnetosheath plasmas. The plasma sheet is a region of hot, slow-moving particles extending to the distant magnetotail. The inner magnetosphere transfers energy to the ionosphere through field-aligned currents (FACs) and plasma flows to the ring current I_{rc}. The ring current occupies part of the plasmasphere but extends out a further distance from the earth. The current is the second largest plasma energy reservoir after the plasma sheet.

As solar wind impinges on the earth's magnetic field, it compresses the field rotates around it at supersonic speed, and creates a boundary called the Magnetopause. The inner region of the magnetopause from which the solar wind is excluded and contains the earth's magnetic field is called the Magnetosphere.

The energetic charges are usually proton and electron are trapped in the Van Allen radiation belts, in regions where they execute complicated trajectories that spiral along the magnetic field lines, and at the same time drift slowly around the earth. (Bittencourt, 2018).

2.4 Magnetohydrodynamics Equations

The Lorentz force controls how charged particles of the solar wind interact with the electromagnetic field.

For a typical particle of charge q and mass m, moving with velocity v, in the presence of electric (E) and magnetic induction (B) fields, the equation of motion is.

$$\frac{d\vec{p}}{\mathrm{dt}} = q\left(\vec{E} + \vec{v} \times \vec{B}\right) \qquad (1)$$

where $\vec{\mathrm{p}} = \mathrm{m}\vec{\mathrm{v}}$ denotes the particle momentum. In theory, it is possible to characterize a plasma's dynamics by solving the equations of motion for each particle of the plasma under the combined influence of the internal fields produced by all the other plasma particles and the external fields applied. If the total number of particles is N, we will have N nonlinear coupled differential equations of motion to solve simultaneously.

The fields where ρ_v, $\vec{J}$, ϵ_0 and μ_0 denote, respectively, the total charge density, the total electric current density, the electric permittivity, and the magnetic permeability of free space.

$$Maxwell's\ equations.$$

$$\vec{\nabla} \cdot \vec{D} = \rho_v \quad (2)$$

$$\vec{\nabla} \cdot \vec{B} = \mu_0 \vec{J} \quad (3)$$

$$\vec{\nabla} \times \vec{E} = -\frac{\partial \vec{B}}{\partial t} \quad (4)$$

$$\vec{\nabla} \times \vec{H} = \frac{\partial \vec{D}}{\partial t} + \vec{J} \quad (5)$$

Magnetohydrodynamics (MHD) couples Maxwell's equations of electromagnetism with hydrodynamics to describe the macroscopic behavior of conducting fluids such as plasmas.

$$Continuity\ equation. \frac{\partial \rho}{\partial t} + \vec{\nabla} \cdot (\rho \vec{v}) = 0 \quad (6)$$

$$Equation\ of\ motion. \rho \left(\frac{\partial}{\partial t} + \vec{v} \cdot \vec{\nabla} \right) \vec{v} = \vec{J} \times \vec{B} - \vec{\nabla} p \quad (7)$$

$$Ohm's\ law. \vec{E} + \vec{v} \times \vec{B} = \eta \vec{J} \quad (8)$$

$\vec{B}$, magnetic field; $\vec{v}$, plasma velocity; $\vec{J}$, current density; $\vec{E}$, electric field; ρ, mass density; p, plasma pressure.

The partial derivative $\frac{\partial \rho}{\partial t}$ refers to the change in density at a single point in space while the divergence of the mass flux $\vec{\nabla} \cdot (\rho \vec{v})$ says how much plasma goes in and out of the region.

The equation of motion $\rho\left(\frac{\partial}{\partial t}+\vec{v}\cdot\vec{\nabla}\right)\vec{v}=\vec{J}\times\vec{B}-\vec{\nabla}p$ has additional forces go on the right-hand side (e.g., gravity). The total derivative is given by $\left(\frac{\partial}{\partial t}+\vec{v}\cdot\vec{\nabla}\right)$ and represents the derivative you take as you follow a parcel of plasma. In a static equilibrium. $\vec{J}\times\vec{B}=\vec{\nabla}p$ when $\vec{J}\times\vec{B}=0$, the plasma is 'force-free'.

The MHD simulations require significant computational resources and provide a detailed analysis but are difficult to interpret. The low order models are computationally less intensive and easier to visualize and interpret. During strong geomagnetic activity, the MHD simulations are more difficult to control because of the strongly nonlinear response of the magnetosphere-ionosphere system. MHD models also do not describe processes in the inner magnetosphere such as the formation of the ring current. To complement the MHD, fluid, and kinetic models, it is very important to have low-dimensional models that attempt to analyze the global or overall behavior of the magnetosphere-ionosphere system by reducing or combining the dynamics of various sections to simulate the interaction between key energy components while being fast and computationally inexpensive.

2.5 Previous Substorm Onset Detection Techniques

Substorm onset simply refers to the dynamic phenomenon surrounding the initiation and observation of substorms in the magnetosphere. An abrupt release of the magnetotail's stored energy occurs during a substorm, causing a variety of phenomena including auroral brightening, magnetic field perturbations, and particle injections.

The exact processes and triggers involved in substorm onset are still a topic of ongoing research and investigation. However, several key features and indicators have been identified about substorm onset and they have been fused into models for determining substorm onset.

2.5.1 Newell and Gjerloev (2011)

This model uses criteria that are based on observations of the interplanetary magnetic field (IMF) and solar wind conditions. These observations include.

1. Southward IMF B_z component which is associated with the reconnection of the earth's magnetic field lines with the IMF, leading to the release of stored energy and substorm onsets.
2. Higher solar wind dynamic pressure and velocity which can compress the earth's magnetosphere and enhance the likelihood of reconnection and substorm onset.
3. IMF clock angle nearing 180 degrees or equivalently near the midnight sector of the magnetosphere.

There have been discrepancies as to whether the B_z turn is important in determining substorm onset. (Maimaiti et al., 2019) suggested that substorms may be internally triggered and a northward turning of B_z is not necessary. They also questioned the role of preconditioning the magnetosphere in terms of tail reconnection during the growth phase; Overturning existing conclusions that current disruption happens before tail reconnection happens during the growth phase.

This study predicts the onset of magnetic substorms using a deep learning-based approach using Solar wind speed (V_x), proton number density (N_p), and IMF components

(B_x, B_y, and B_z) as input to the system to forecast the occurrence probability of onset over 1hr duration using Mag data between 1997 and 2017. Solar wind and IMF data were obtained from the ACE spacecraft. The analysis is limited to only substorms with SML index < -3000 nT (Newell & Gjerloev, 2011).

Substorm onset detection rules by Newell and Gjerloev (2011).

- $SML(t_0 + 1) - SML(t_0) < -15\ nT$
- $SML(t_0 + 2) - SML(t_0) < -30\ nT$
- $SML(t_0 + 3) - SML(t_0) < -45\ nT$
- $\sum_{i=4}^{29} SML(t_0 + i) - SML(t_0) < -100\ nT$

The interval between t and t1=1min and the minimum permitted time between two consecutive onsets is 20min and a drop in SML intimates substorm onset.

In the Ionosphere, substorm expansion phases are accompanied by the brightening and expansion of the nightside aurora. During the growth phase which is estimated to last 30-90min, magnetic flux is added to the magnetotail lobes through reconnection at the dayside magnetopause. As the lobe magnetic flux increases, aurora oval moves equatorward, and plasma temperature increases.

The Substorm Onset is simply the onset of the expansion phase, and it explains the brightening of the auroral intensity. The end of the expansion phase is the start of the recovery phase, and it is indicated by the reduction of the aurora intensity. While most isolated substorms follow the Growth-Expansion-Recovery paradigm, there exist some events that go against this paradigm and to ascertain this, the author used substorm onset lists from space data, ground-based auroral imagers, and ground-based magnetometers.

2.5.2 SOPHIE Model. Forsyth et al., (2015)

The SOPHIE technique (Forsyth et al., 2015) identifies the substorm growth, expansion, and recovery phase with the growth phase (Potential) being the times outside the expansion and recovery phase. SOPHIE is used to categorize substorms into different phases based on their magnetic signatures. The growth phase involves the accumulation of magnetic energy in the magnetotail. The expansion phase is characterized by the rapid release of this stored energy leading to auroral brightening and geomagnetic disturbances. The recovery phase is when the magnetosphere returns to a more stable state after a substorm.

All these are based on the time derivatives of filtered SML data with assumptions being made that negative changes in SML beyond a user-specified percentile level are indicative of substorm expansion phases and positive changes in SML are due to substorm recovery phases. According to this method, the recovery phase doesn't have to happen immediately after the expansion phase. The time derivative of SML, $\frac{dSML}{dt}$ is being calculated using three-point Lagrangian interpolation such that $\frac{dSML}{dt} < 0$ (expansion percentiles, EPs) and $\frac{dSML}{dt} > 0$ (recovery percentiles, RPs).

This model considered all non-expansion and non-recovery times to be growth phases with the argument metric that all solar wind functions are nonzero for all but purely northward IMF. Based on this, Substorm phases are identified by.

1. Low pass filtering of the data with a 30-minute cut-off to remove the effect of ULF waves.

2. Calculating the time derivative of SML ($\frac{dSML}{dt}$) using a three-point Lagrangian interpolation.
3. Calculating percentiles of $\frac{dSML}{dt} < 0$ (expansion percentiles) and $\frac{dSML}{dt} > 0$ (Recovery Percentiles).

   EP < $\frac{dSML}{dt}$ < 0, Expansion phase where EP-Threshold

   0 < $\frac{dSML}{dt}$ < EP, Recovery phase. Every other interval represents a Growth Phase.

2.6 WINDMI Model

The WINDMI model (Spencer et al., 2009) is a pivotal component of this research, serving as a physical model that experimentally validates real-life scenarios of magnetosphere-ionosphere coupling. This plasma physics-based model relies on a fundamental concept known as the solar wind dynamo voltage, V_{sw}, which is generated through a specific solar wind-magnetosphere coupling function. This voltage acts as the driving force behind the model's operation.

The model is structured around a system of eight ordinary differential equations, and these equations play a critical role in describing the transfer of power throughout distinct regions within the magnetosphere. The areas covered by these equations include the geomagnetic tail, the ionosphere, and the ring current. These components collectively constitute a complex and dynamic system, each with its unique characteristics and interactions.

To derive the WINDMI model, certain assumptions are made regarding the configuration of the magnetosphere. The equations that define the model are meticulously

constructed to account for the intricacies of magnetospheric dynamics, ensuring that they accurately represent the complex interplay of energy flows, currents, and magnetic fields within this vast region.

These equations, central to the WINDMI model, serve as a foundation for the research, enabling deep exploration of substorm dynamics, initiation criteria, and their impacts on the magnetosphere-ionosphere system. The model's operational principles and equations are a cornerstone of this study, facilitating a comprehensive understanding of the physical processes at work in the dynamic space environment.

WINDMI model equations.

$$L\frac{dI}{dt} = V_{SW}(t) - V + M\frac{dI_1}{dt} \tag{9}$$

$$C\frac{dV}{dt} = I - I_1 - I_{ps} - \Sigma V \tag{10}$$

$$\frac{3}{2}\frac{dp}{dt} = \frac{\Sigma V^2}{\Omega_{cps}} - \mu_0 p K_{\parallel}^{\frac{1}{2}}\Theta(u) - \frac{pVA_{eff}}{\Omega_{cps}B_{tr}L_y} - \frac{3p}{2\tau_E} \tag{11}$$

$$\frac{dK_{\parallel}}{dt} = I_{ps}V - \frac{K_{\parallel}}{\tau_{\parallel}} \tag{12}$$

$$L_1\frac{dI_1}{dt} = V - V_1 + M\frac{dI}{dt} \tag{13}$$

$$C_1\frac{dV_1}{dt} = I_1 - I_2 - \Sigma_1 V_1 \tag{14}$$

$$L_2\frac{dI_2}{dt} = V_1 - (R_{prc} + R_{A2})I_2 \tag{15}$$

$$\frac{dW_{rc}}{dt} = R_{prc}I_2^2 + \frac{pVA_{eff}}{B_{tr}L_y} - \frac{W_{rc}}{\tau_{rc}} \tag{16}$$

This model has been employed on some events and the output can be manipulated based on different conditions which may include.

Analysis of the data, combined with theoretical study of the plasma and particle processes in the solar terrestrial region, has resulted in different physical models that attempt to explain the various phenomena observed. The complexity and diversity of physical phenomena that appear have resulted in multi-scale modeling of the sun-earth processes. On one end, we have Magneto-hydrodynamics (MHD) simulations that divide a certain region into small grid cells and apply the full set of ideal plasma fluid equations to every cell (Zhang et al., 2019).

These methods attempt to analyze the plasma flows and the propagation of disturbances within the magnetosphere as accurately as possible and with high spatial and temporal resolution. On the other end, some low-order models attempt to analyze the global or overall behavior of the magnetosphere-ionosphere system by reducing or combining the dynamics of various sections to simulate the interaction between key energy components. These models include some higher-order physics such as instabilities in certain regions of the magnetosphere. An example of a low-order physics model is the WINDMI model of (Horton et al., 1998) (Horton et al., 1998) and (Smith et al., 2000).

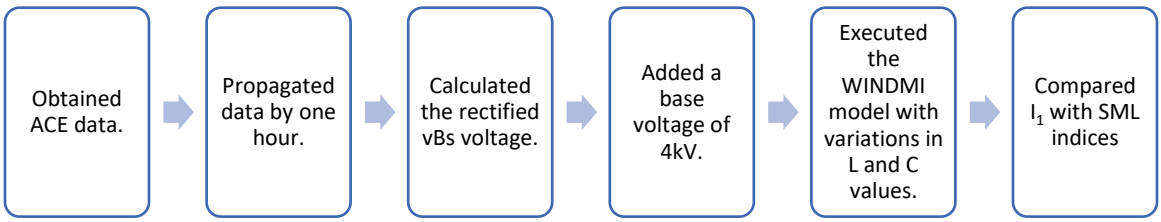

Figure 2. Flowchart of the methodology for processing and analyzing ACE data in the study of substorms.

The methodology for substorm analysis involves several key steps that offer distinct advantages over the conventional approach using Magnetohydrodynamics (MHD).

1. Utilizing Solar Wind VBs Input with Steady Magnetospheric Convection. The first approach involves employing solar wind VBs (velocity and magnetic field) as input data, assuming steady magnetospheric convection. This method is compared to the conventional use of the negative of the SuperMAG AL (SML) index.
2. Utilizing Solar Wind VBs Input with Substorm Trigger Activation. In the second approach, solar wind VBs data is utilized with the substorm trigger turned on, offering a unique perspective when contrasted with the conventional method using the negative SML index.
3. Leveraging the Newell Coupling Function with Steady Magnetospheric Convection. The third step incorporates the Newell coupling function as the input data, again assuming steady magnetospheric convection. This alternative approach is compared to the traditional use of the negative SML index.
4. Using the Newell Coupling Function with Substorm Trigger Activation. Finally, the fourth approach implements the Newell coupling function as input data with the substorm trigger activated. This method provides an innovative viewpoint when compared to the conventional use of the negative SML index.
5. These distinct methodologies offer a unique perspective on substorm analysis, presenting advantages over the conventional MHD approach. By exploring various input data sources and activation conditions, this research seeks to enhance our understanding of substorm dynamics and their impacts on the magnetosphere-ionosphere system.

2.7 Chapter Summary

Specific patterns and features observed in auroral activity, along with distinctive electrojet current signatures can serve as reliable initiation criteria for the onset of geomagnetic substorms. Identifying important factors and key criteria that might aid in predicting the occurrence and timing of substorm requires a thorough analysis of observational data, notifying the correlation and disparity in the data with an in-depth understanding of individual criteria. WINDMI model which is a low-order model that analyzes the overall behavior of the magnetosphere-ionosphere system by combining the dynamics of various sections to simulate the interaction between key energy components.

The input data is derived from the Advanced Composition Explorer (ACE) satellite measurements of solar wind plasma quantities, while the output is compared to the SuperMAG index measured on the earth's surface.

CHAPTER III

EVENT-BASED AURORAL OBSERVATIONS AND ELECTROJET CURRENT SIGNATURES

Electrojet current signatures refer to distinctive patterns of electric current flows within the Earth's ionosphere, particularly in high-latitude regions. Electrojets are narrow bands of electrical currents that flow horizontally within the ionosphere, and they play a crucial role in understanding the complex interactions within Earth's space environment. There are two primary electrojets of significance. the auroral electrojet and the mid-latitude electrojet. These electrojets exhibit unique current signatures and behaviors.

Auroral Electrojets. These electrojets are primarily found in the high latitude auroral zone, typically ranging from 60° to 80° magnetic latitude. Within this region, currents flow in a westward direction, which is opposite to the Earth's rotation.

The formation and behavior of these electrojets are a consequence of the interaction between the solar wind and the Earth's magnetosphere. They are intimately linked to geomagnetic storms and disturbances in the Earth's magnetic field. The electric currents associated with electrojets generate magnetic variations on the Earth's surface, playing a significant role in space weather phenomena. These variations can impact various technological systems on Earth, including satellite communications, navigation systems, and power grids.

Observing and studying electrojet current signatures is typically accomplished using ground-based magnetometers and instruments on satellites or high-altitude balloons. These observations provide invaluable data for scientists and researchers, enabling them to monitor and comprehend the intricate interactions between the solar wind, the Earth's magnetic field, and the ionosphere. This understanding contributes to our knowledge of space weather and its implications for technology on Earth.

Numerous scholars have contributed to the study of electrojet current signatures, with notable researchers such as (Forsyth et al., 2015; Frey et al., 2004; Newell et al., 2010; Newell & Gjerloev, 2011; Werner et al., 2023) developing criteria based on their investigations. As we progress in this discussion, we will delve into these criteria and their significance, concerning the respective years of their research.

3.1 Existing Lists of Substorm Onsets

While there has not been an exact prediction model for substorm onset due to the complex and variable nature of these phenomena, ongoing research and advancements in data analysis techniques offer hope for improved prediction capabilities in the future. Accurate substorm prediction carries significant implications for space weather forecasting and the protection of satellites and power grids on Earth. To achieve this, it is essential to thoroughly investigate existing models that have made predictions based on different criteria using ground-based measurements and auroral observations (Partamies et al., 2011, 2013).

The onset of substorms occurs along the magnetic field lines of the inner proton plasma sheet and is initially observed in the aurora as beading along the onset aurora arc,

located near the equatorward boundary of the auroral oval. The growth of these onset waves and the presence of large amplitude electric field oscillations indicate an abrupt transition from a stable to an unstable state, leading to onset. This transition to instability is triggered by the intrusion of a low-entropy flow burst or channel, often referred to as a plasma bubble, into the inner plasma sheet. These flow bursts are marked in the auroral oval by the initiation of a poleward boundary intensification (PBI) that subsequently evolves into an auroral streamer.

Plasma flows associated with these and other PBIs are generally linked to enhanced reconnection at the distant tail neutral line. This reconnection is typically triggered by an incoming flow channel from the polar cap.

In this study, the statistics of the output from different models were compared with the WINDMI model to establish common ground and identify an effective and efficient prediction model for substorm onset. This research aims to contribute to our understanding of the complex dynamics of substorms and to provide valuable insights into space weather forecasting and its practical applications in safeguarding vital technological systems on Earth.

The events that were studied are.

1. March 09, 2008
2. January 07, 2000
3. April 24, 2003
4. August 09, 2016
5. April 26, 2013, etc.

These events were picked based on the availability of data from the ground as well as satellite observations. All of THEMIS deployed satellites showed activities for these days. Themis orbits in GSM X and Y coordinates are shown below.

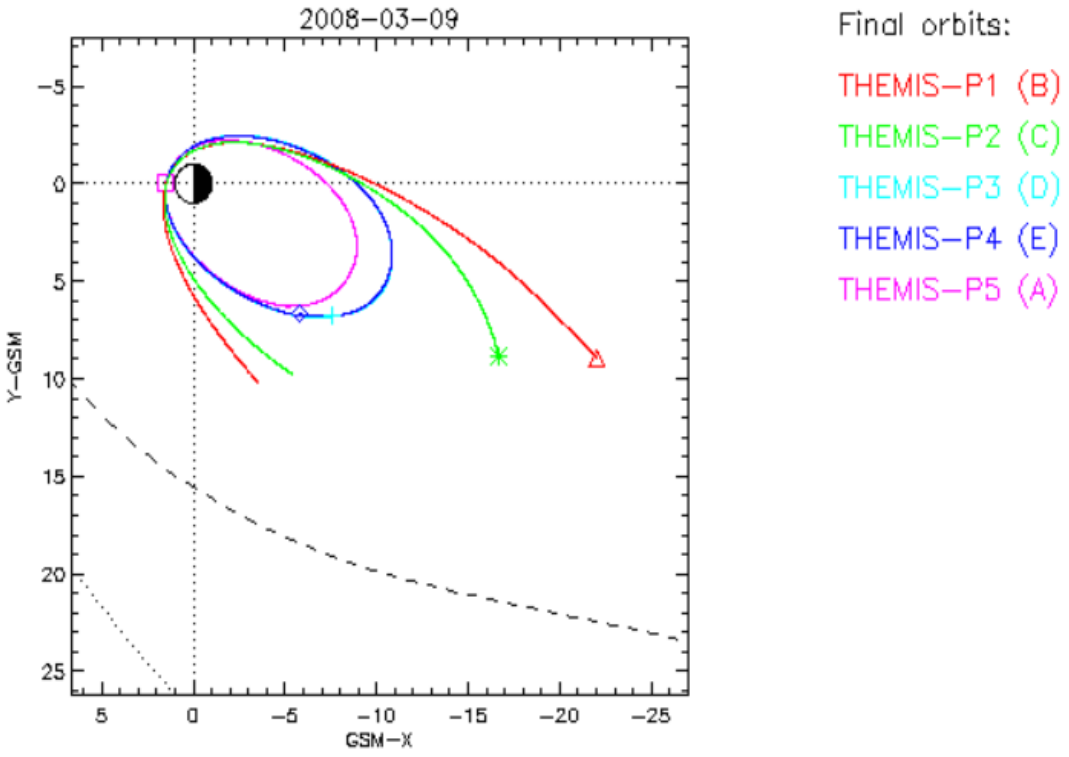

Figure 3. THEMIS orbits shown in GSM X and Y coordinates.

Figure 3 displays the final orbits of the satellites before they deviated from their planned paths. Throughout the mission, these satellites captured numerous images of auroral brightening, indicative of substorm events.

The THEMIS mission consists of multiple spacecraft designed to study magnetospheric substorms and the auroral phenomena associated with them. Each

THEMIS spacecraft is positioned at a different location in space to provide a multipoint measurement capability to study the dynamics of substorms. The spacecraft are deployed such that they are at slightly different distances from the Earth, along the magnetotail.

THEMIS is a NASA satellite mission with the primary goal of studying the dynamics and processes within Earth's magnetosphere. THEMIS consists of a constellation of five identical satellites equipped with various scientific instruments, including magnetometers and particle detectors. These satellites collect data directly from space, providing detailed information on the magnetospheric and ionospheric conditions during geomagnetic events. THEMIS is a constellation of five similar spacecraft carrying a variety of scientific equipment, such as particle detectors and magnetometers. By gathering information straight from space, these satellites can provide comprehensive details on the magnetospheric and ionospheric conditions during geomagnetic occurrences.

SuperMAG is a collaborative network of ground-based magnetometer stations that exchanges and makes available real-time data on fluctuations in the Earth's magnetic field. The data from SuperMAG stations contribute to a global perspective on space weather conditions, such as geomagnetic storms and substorms. While SuperMAG focuses on monitoring the magnetic field from multiple ground-based locations, it does not have a satellite mission. The veracity of SuperMAG data makes this research possible as the end goal is to compare the field-aligned current output of the WINDMI model and its slope with that of SML.

The SML is an index that quantifies the level of geomagnetic activity and disturbance at an instant of time and location. It is calculated based on measurements of

the horizontal component of the magnetic field (H) obtained from various SuperMAG magnetometer stations. It represents the deviation of the magnetic field from its quiet time reference level. The criteria of most ground-based models depend on SML. The time-dependent plot of the SML index at the different phases of substorm onsets is shown below.

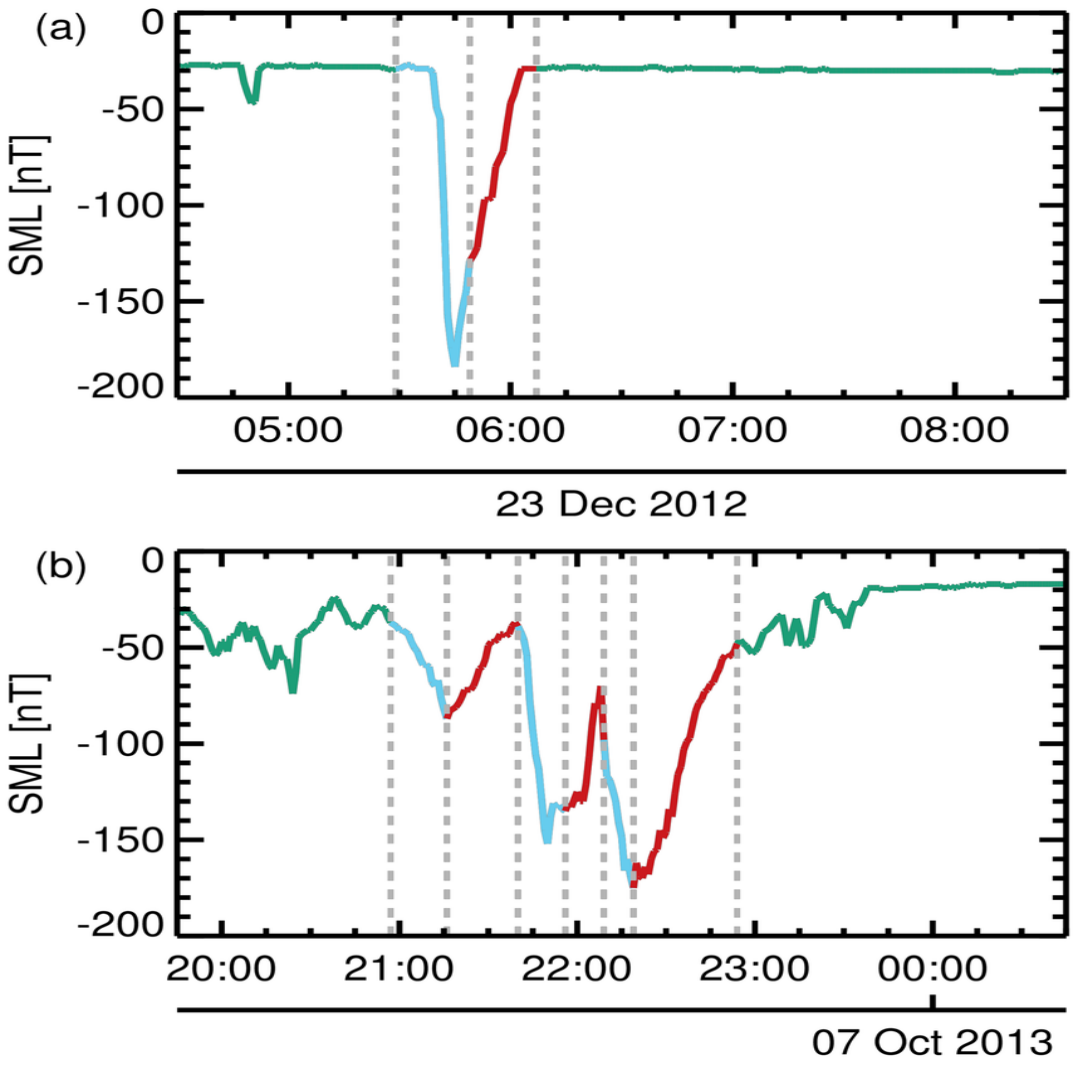

Figure 4. Time-dependent plot of the SML index(nT) illustrating stand-alone and interconnected substorms.

In Figure 4, substorm phases are color-coded based on the Substorm Onsets and Phases from Indices of the Electrojet technique. Green represents the growth phase, blue indicates the expansion phase, and red designates the recovery phase. Vertical gray dashed lines mark the initiation times of each phase.

3.1.1 Newell and Gjerloev (2011) Substorm List

The (Newell & Gjerloev, 2011) SML data for substorm onset depends on the Newell Model. This model uses criteria that are based on observations of the interplanetary magnetic field (IMF) and solar wind conditions. These observations include.

1. Southward IMF B_z component**.** This is a negative IMF Bz component that is associated with the reconnection of the earth's magnetic field lines with the IMF, leading to the release of stored energy and substorm onsets.
2. Higher solar wind dynamic pressure and velocity**.** This is an increase in solar wind dynamic pressure which can compress the earth's magnetosphere and enhance the likelihood of reconnection and substorm onset.
3. Increased electrojet currents which corresponds to enhanced magnetospheric convection and IMF clock angle nearing 180 degrees or equivalently near the midnight sector of the magnetosphere.

According to (Newell & Gjerloev, 2011), Onsets are identified at time=t_0 when four conditions are satisfied.

- $SML(t_0 + 1) - SML(t_0) < -15\ nT$
- $SML(t_0 + 2) - SML(t_0) < -30\ nT$

- $SML(t_0 + 3) - SML(t_0) < -45\ nT$
- $\sum_{i=4}^{29} SML(t_0 + i) - SML(t_0) < -100\ nT$

The conditions explain the rate of change of SML ($\frac{dSML}{dt}$). Onset prediction using the Newell model for the listed dates is noted. All the observations are further discussed.

3.1.2 Forsyth et al. (2015) Substorm List

This model employs the Sophie technique which seeks to identify substorm expansion, recovery, and potential growth phase (times outside the expansion and recovery phases) based on the time derivatives of filtered SML data. When these derivatives exceed a set percentile of the yearly distribution, the data is flagged as an expansion phase. Recovery phases are similarly identified, but the corresponding percentile is found iteratively such that the number of expansion and recovery phases is similar. Short phases, between expansion and recovery phases, are reclassified and further processing is applied to account for the Gibbs effect when filtering the data. Finally, the rates of change of SML and SMU are compared, and times when these are similar are flagged as potentially due to enhanced convection. Note that this technique does not specify minimum or maximum phase lengths, nor that the phases occur in a specific order.

According to Forsyth, Substorms are the elemental dissipative events in the coupled solar wind-magnetosphere-ionosphere system that process approximately 10^{15}J of captured solar wind energy during their lifetime, and substorm expansion phases are accompanied by depolarization of the magnetic field, injection of energetic particles into the inner magnetosphere, a reduction of magnetic flux within the magnetotail lobes and a

diversion of the cross-tail current into the ionosphere. (Forsyth et al., 2015) employed a nonparametric approach to identify substorms based on the exceedance of a percentile in the rate of change of SML. Their method involved identifying the expansion and recovery phases, considering that expansion phases could transition into steady magnetospheric convection events. Initially, the data were low pass filtered to mitigate ULF wave effects, and specific thresholds based on percentile data were used to determine the expansion and recovery phases.

3.1.3 Frey et al. (2004 & 2006) Substorm List

The Frey substorm list was generated through the systematic examination of auroral brightening using image observations. This comprehensive observation process primarily relied on the analysis of Far Ultraviolet (FUV) data, with a particular emphasis on the utilization of Wideband Imaging Camera (WIC) images, known for their superior spatial resolution. To identify and categorize substorms, a set of specific criteria was rigorously applied.

1. Substorms were considered when there was a conspicuous and localized intensification of auroral luminosity. This observable phenomenon served as an initial indicator of substorm activity.
2. The observed auroral brightening had to exhibit a significant expansion, reaching the poleward boundary of the auroral oval. This expansion also needed to manifest azimuthally in local time for a minimum duration of at least 20 minutes, signifying the dynamic and evolving nature of the substorm event.

3. Substorm onsets were considered as separate and distinct events if at least 30 minutes had elapsed since the occurrence of the previous onset. This criterion helped ensure the differentiation of individual substorm events within the dataset.

Through the meticulous application of these criteria, the Frey substorm list was compiled, providing a valuable resource for the study and analysis of substorm activity in the Earth's magnetosphere.

3.1.4 Ohtani and Gjerloev (2020) substorm list

The core objective of this technique is to confidently identify isolated substorms, characterized by their distinct substorm features and behaviors. Isolated substorms represent individual substorm events that occur independently of one another, rather than forming part of a continuous sequence of geomagnetic disturbances. These events are marked by abrupt and significant increases in both geomagnetic and auroral activities, and their onset is typically short-lived. The key factor underlying the occurrence of isolated substorms is the release of energy previously stored in the Earth's magnetotail.

To identify these isolated substorms, a set of six criteria is employed. Each of these criteria is rooted in classical substorm characteristics, as documented in the extensive substorm literature. By adhering to these criteria, researchers can confidently discern isolated substorms from other geomagnetic events and disturbances.

Furthermore, (Tsurutani et al., 2023) introduced a modified technique for identifying isolated substorms, building upon the foundation laid by (Newell & Gjerloev, 2011). In their method, Ohtani and Gjerloev implemented a smoothing process on the SML index to effectively filter out small-scale variations. Their approach focused on

identifying the growth phase slope, which exhibits a small negative slope that culminates in an onset break, creating a noticeable knee in the SML curve. Additionally, they observed that the expansion phase slope was notably steeper in comparison to the growth phase slope. The smoothing process and conditions that begat the substorm lists based on this criterion are shown below.

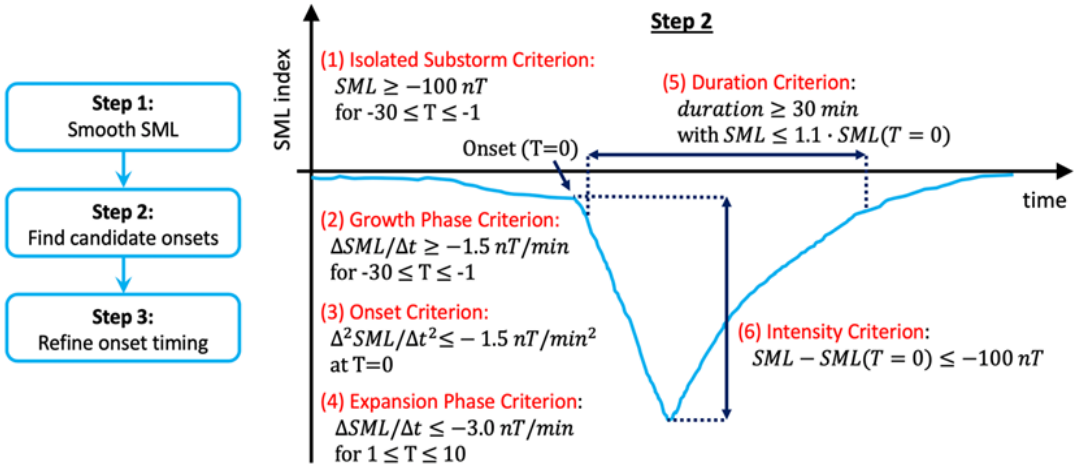

Figure 5. Schematic explanation of onset detection by (Ohtani & Gjerloev, 2020)

In this modified technique, Ohtani and Gjerloev retained the criteria established by (Newell & Gjerloev, 2011) which require the substorm's duration to exceed 30 minutes and mandate that the average value of the SML index during the substorm duration should be less than -100 nT. This refined approach enhances the accuracy and reliability of isolated substorm identification, contributing to a deeper understanding of these distinctive geomagnetic events.

The depicted data reflects the diligent efforts of these researchers in identifying and cataloging substorm onset events using their respective criteria. Substorm onsets represent significant and dynamic occurrences within the Earth's magnetosphere and are integral to our understanding of space weather phenomena. The auroral imaging-based substorm lists proposed by Liou were disregarded because of inconsistencies in the data availability.

The availability of substorm onset data based on the aforementioned rules is shown below.

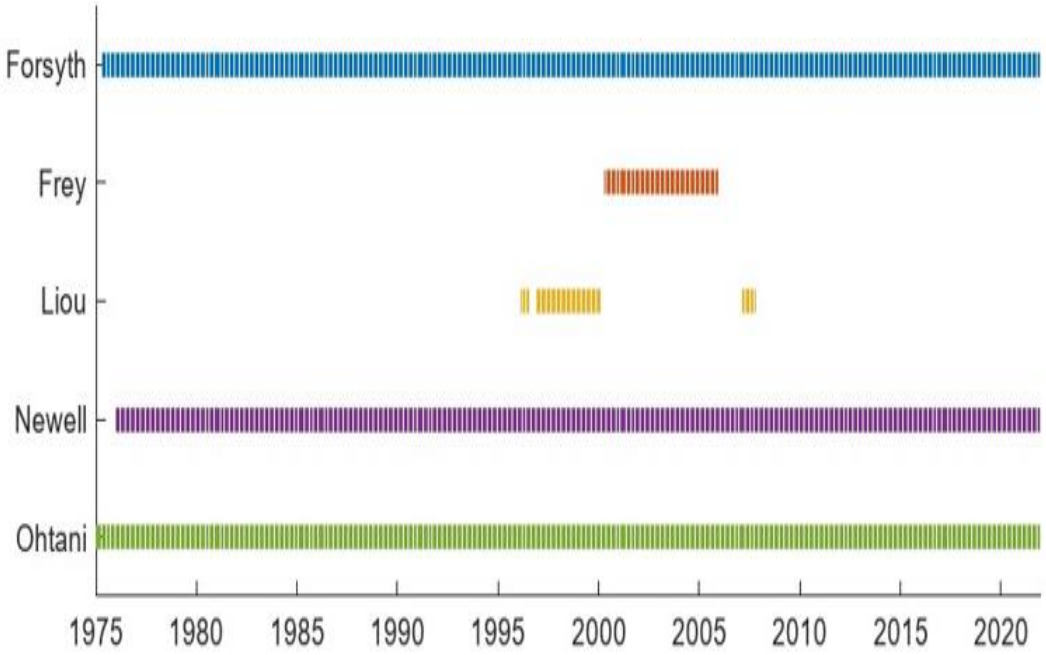

Figure 6. Availability of substorm onset data based on criteria from publications by Availability of substorm onset data based on criteria from publications by (Forsyth et al., 2015; Frey et al., 2004; Newell et al., 2010; Newell & Gjerloev, 2011; Ohtani & Gjerloev, 2020)

Figure 6 above provides an overview of the availability of substorm onset data spanning the period from 1975 to 2020, as sourced from the SuperMAG website. The data presented in this figure is derived from distinct criteria outlined in publications by various researchers, including (Forsyth et al., 2015; Frey et al., 2004; Newell et al., 2010; Newell & Gjerloev, 2011; Ohtani & Gjerloev, 2020).

The figure serves as a visual representation of the temporal coverage and distribution of substorm onset data, offering insights into the periods and events that have been extensively studied based on the criteria provided by the aforementioned researchers. It highlights the contribution of each research group to the collective knowledge of substorm activities and serves as a valuable resource for the broader scientific community engaged in magnetospheric and space weather research. The figure also underscores the comprehensive nature of the data available for the analysis and comparison of substorm onset events over several decades.

There is a break in availability of data for some models as shown in the images below. Frey and Liou whose lists are based on auroral imaging have substorm onset lists only for a few years, thus, the focus of this data comparison will be on the substorm list based on magnetic indices with a focus on the following techniques. (Forsyth et al., 2015; Newell & Gjerloev, 2011) and (Ohtani & Gjerloev, 2020) (Isolated Substorms).

Tables 1 through 5 present the onset times for magnetic indices across various events. These tables depict a range of onset patterns, including intersections on some days, proximity on others, and more significant temporal differences on certain occasions. Analyzing the reasons behind these variations is essential in the context of our research, contributing to our understanding of the dynamics of these magnetic indices and

their relationships. This scientific investigation aims to provide insights into the observed patterns and their implications in the field of magnetospheric research.

Table 1. Substorm onsets detected on 07 Jan 2000 using various techniques. Onsets within 15 minutes of each other are grouped in the same row, indicating they correspond to the same substorm.

Substorm No	Forsyth	Liou	Newell	Ohtani
1	1/7/2000 0.34	1/7/2000 0.31	1/7/2000 0.32	1/7/2000 0.28
2		1/7/2000 0.48		
3	1/7/2000 1.35		1/7/2000 1.29	
4				1/7/2000 3.24
5	1/7/2000 3.41			
6				1/7/2000 4.44
7	1/7/2000 5.36			
8	1/7/2000 7.33			
9	1/7/2000 9.28		1/7/2000 9.35	1/7/2000 9.32
10	1/7/2000 14.16		1/7/2000 14.22	1/7/2000 14.24
11	1/7/2000 16.06	1/7/2000 16.05	1/7/2000 16.06	1/7/2000 16.04
12	1/7/2000 17.14		1/7/2000 17.19	
13		1/7/2000 18.09		
14		1/7/2000 18.16		
15	1/7/2000 18.28		1/7/2000 18.35	
16	1/7/2000 19.26		1/7/2000 19.26	
17	1/7/2000 20.37		1/7/2000 20.37	

Table 2. Substorm onsets detected on 24 April 2003 using various techniques. Onsets within 15 minutes of each other are grouped in the same row, indicating they correspond to the same substorm.

Substorm #	Forsyth	Frey	Newell
1	4/24/2003 5.52		4/24/2003 5.51
2			4/24/2003 6.37
3	4/24/2003 6.54		
4	4/24/2003 9.07		4/24/2003 8.58
5	4/24/2003 10.04		4/24/2003 10.03
6	4/24/2003 11.28		
7	4/24/2003 12.29		4/24/2003 12.28
8	4/24/2003 13.17		4/24/2003 13.22
9	4/24/2003 14.40		4/24/2003 14.37
10		4/24/2003 14.59	
11	4/24/2003 16.49		4/24/2003 16.46
12	4/24/2003 17.26	4/24/2003 17.21	
13	4/24/2003 18.13		
14			4/24/2003 18.52
15	4/24/2003 19.17		4/24/2003 19.16
16			4/24/2003 19.55
17	4/24/2003 20.55		4/24/2003 20.50
18	4/24/2003 21.38		4/24/2003 21.38
19			4/24/2003 23.59

Table 3. Substorm onsets detected on March 09, 2008, using various techniques. Onsets within 15 minutes of each other are grouped in the same row, indicating they correspond to the same substorm.

Substorm #	Forsyth	Newell	Ohtani
1	3/9/2008 1.08		3/9/2008 1.16
2		3/9/2008 1.46	
3		3/9/2008 2.07	
4	3/9/2008 2.33		
5		3/9/2008 3.50	
6	3/9/2008 4.56	3/9/2008 4.52	
7		3/9/2008 5.14	
8	3/9/2008 6.15	3/9/2008 6.22	
9	3/9/2008 6.46	3/9/2008 6.46	
10		3/9/2008 7.08	
11	3/9/2008 7.16		
12	3/9/2008 8.25		
13	3/9/2008 9.37	3/9/2008 9.37	
14		3/9/2008 10.05	
15	3/9/2008 11.00	3/9/2008 11.00	
16		3/9/2008 12.57	3/9/2008 12.58
17	3/9/2008 13.36		
18	3/9/2008 16.30		
19	3/9/2008 17.20	3/9/2008 17.20	3/9/2008 17.22
20	3/9/2008 18.54		
21	3/9/2008 20.32		
22		3/9/2008 20.51	3/9/2008 20.51
23	3/9/2008 21.33	3/9/2008 21.33	
24		3/9/2008 21.59	

Table 4. Substorm onsets detected on April 26, 2013, using various techniques. Onsets within 15 minutes of each other are grouped in the same row, indicating they correspond to the same substorm.

Substorm #	Forsyth	Newell	Ohtani
1	4/26/2013 2.08		4/26/2013 2.15
2		4/26/2013 2.48	
3		4/26/2013 3.17	
4	4/26/2013 6.41	4/26/2013 6.52	
5			4/26/2013 8.25
6	4/26/2013 10.57	4/26/2013 10.57	
7	4/26/2013 11.30	4/26/2013 11.30	
8	4/26/2013 14.32	4/26/2013 14.44	
9		4/26/2013 15.06	
10	4/26/2013 15.50		
11	4/26/2013 16.42		
12	4/26/2013 18.27		
13		4/26/2013 18.42	4/26/2013 18.51
14		4/26/2013 19.09	
15			4/26/2013 22.10

Table 5. Substorm onsets detected on August 09, 2016, using various techniques. Onsets within 15 minutes of each other are grouped in the same row, indicating they correspond to the same substorm.

Substorm #	Forsyth	Newell	Ohtani
1	8/9/2016 3.14	8/9/2016 3.14	8/9/2016 3.13
2		8/9/2016 4.03	
3	8/9/2016 9.21	8/9/2016 9.24	
4	8/9/2016 12.42	8/9/2016 12.42	
5	8/9/2016 15.21	8/9/2016 15.20	
6	8/9/2016 21.01		8/9/2016 20.57
7	8/9/2016 22.01	8/9/2016 22.06	
8	8/9/2016 23.47		

3.2 Magnetic indices for varying events

The magnetic indices encompass a set of parameters, including the auroral electrojet indices (AE), ring current indices, and solar wind parameters. Among these parameters, the solar wind parameters assume paramount significance in substorm prediction. These parameters may encompass numerous factors, such as magnetic field strength, solar wind speed, dynamic pressure, plasma density, clock angle, and others, all of which can be observed in either Geocentric Solar Magnetospheric (GSM) or Geocentric Solar Ecliptic (GSE) coordinates.

The GSM coordinate system is defined with respect to the Earth's dipole magnetic field axis, with one of its axes aligned towards the Earth's non-magnetic pole and the

other directed along the line connecting the Earth to the Sun. These parameters play a pivotal role in the prediction of substorm onset, particularly when observed in GSM coordinates. This coordinate system proves especially valuable for investigating the intricate interactions among the solar wind, the Earth's magnetosphere, and the ensuing phenomena, such as geomagnetic storms and substorms. For instance, on March 9, 2008, a day marked by heightened geomagnetic activity, a substantial number of events were recorded. Newell captured sixteen events, Forsyth identified fifteen, and as per Ohtani and Gjerloev's findings, four isolated substorms occurred on that day. A glimpse of the solar wind parameters for this date is provided in the figure below.

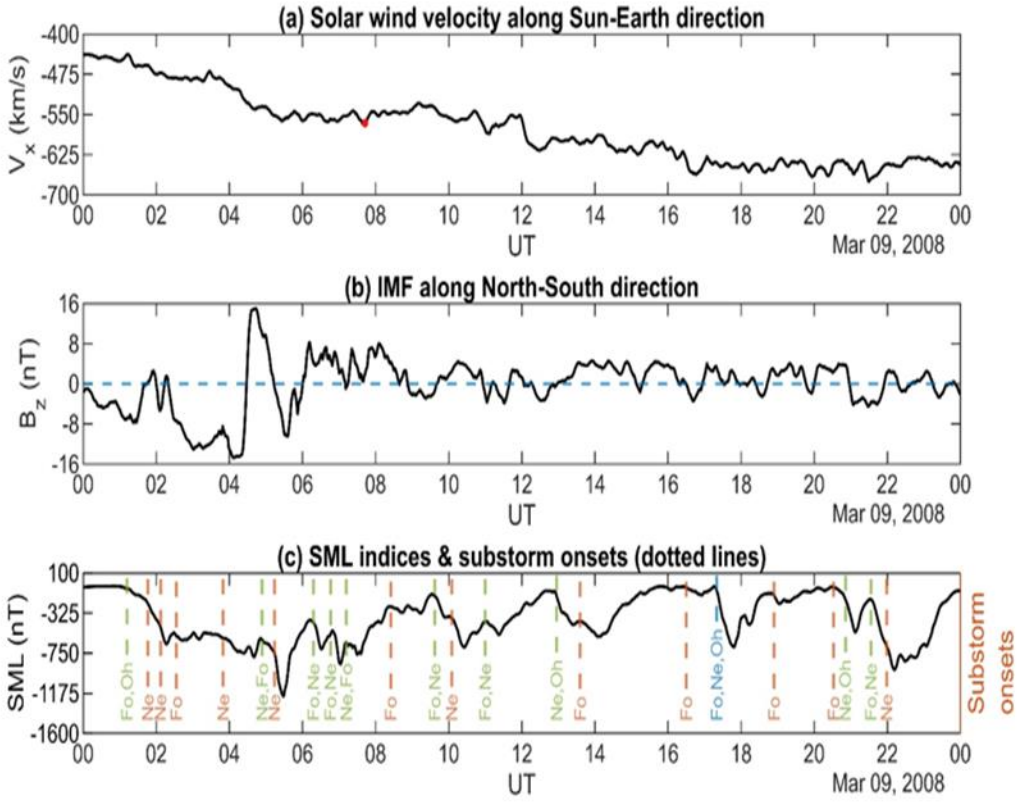

Figure 7. Background Magnetic Conditions on March 9, 2008 (Supermag Indices, n.d.)

Panel (a) displays the solar wind velocity along the Sun-Earth direction. Panel (b) presents the Interplanetary Magnetic Field (IMF) along the North-South direction. Panel (c) showcases the SuperMAG-based SML indices, and the associated substorm onset times as determined by various techniques. These magnetic conditions as shown in Figure 7 offer insights into the geomagnetic environment on the specified date. Two key factors about the solar wind, a persistent stream of charged particles (plasma) emitted from the Sun, are its speed and the intensity of its magnetic field. These parameters are important in predicting space weather events.

The solar wind and the magnetic field parameters are essential for understanding the interactions between the solar wind and the earth's magnetosphere. The solar wind parameters provide insights into plasma dynamics. From the plots, the behaviors of each solar wind parameter as well as the magnetic field parameters are unique and thus the driving effect on the WINDMI model becomes unique. This uniqueness is the reason for the varying outputs of the model. It is important to make inferences from our analysis. Comparing the substorm onset time of the WINDMI model with that of other indices can help shed light on the disparity between criteria and how the criteria influence output. The substorm list used in this project are days with numerous events which will make the inference of our analysis worthwhile as no previous study has specifically compared the calculated onset times with previously published lists of substorm onset.

The solar wind parameters are instrumental in the prediction of substorm onset, playing a pivotal role in this process. Observing these parameters in Geocentric Solar Magnetospheric (GSM) Coordinates is of paramount importance, as it provides a valuable perspective for studying the intricate interactions between the solar wind, the

Earth's magnetosphere, and the associated phenomena, such as geomagnetic storms and substorms.

The choice of GSM coordinates offers unique advantages, enabling a comprehensive examination of the relationships and dynamics within this system. This approach is particularly advantageous when seeking to understand the complex interplay between the solar wind and the Earth's magnetosphere, shedding light on the factors influencing geomagnetic disturbances, including the onset of substorms. Statistical analysis of true data will give insight into the relationship between the solar wind and magnetic field properties concerning substorm onset.

The relationship between SML and its gradient for all substorm onsets taken for this research is shown below. SML is divided into 10 bins, ranging from -1400 to 0 nT, with labels corresponding to the lower limit of each bin and a bin width of 140 nT.

There are more onset times around SML values of -280 nT to -840 nT at a lower gradient of -30 nT/min to -90 nT/min. The onset distribution is more concentrated at lower gradient and lower SML index. For dSML/dt, See Figure 8 below, number of bins is also 10, covering a total range of -300 to 0 nT/min, with each bin spanning 30 nT/min.

The heatmaps depict the counts of substorm onsets within the respective bins. SML and dSML/dt values are calculated based on the maximum values within a 30-minute window before and after the detected substorm onsets, considering substorm occurrences within the 30-minute boundaries as time-period limits.

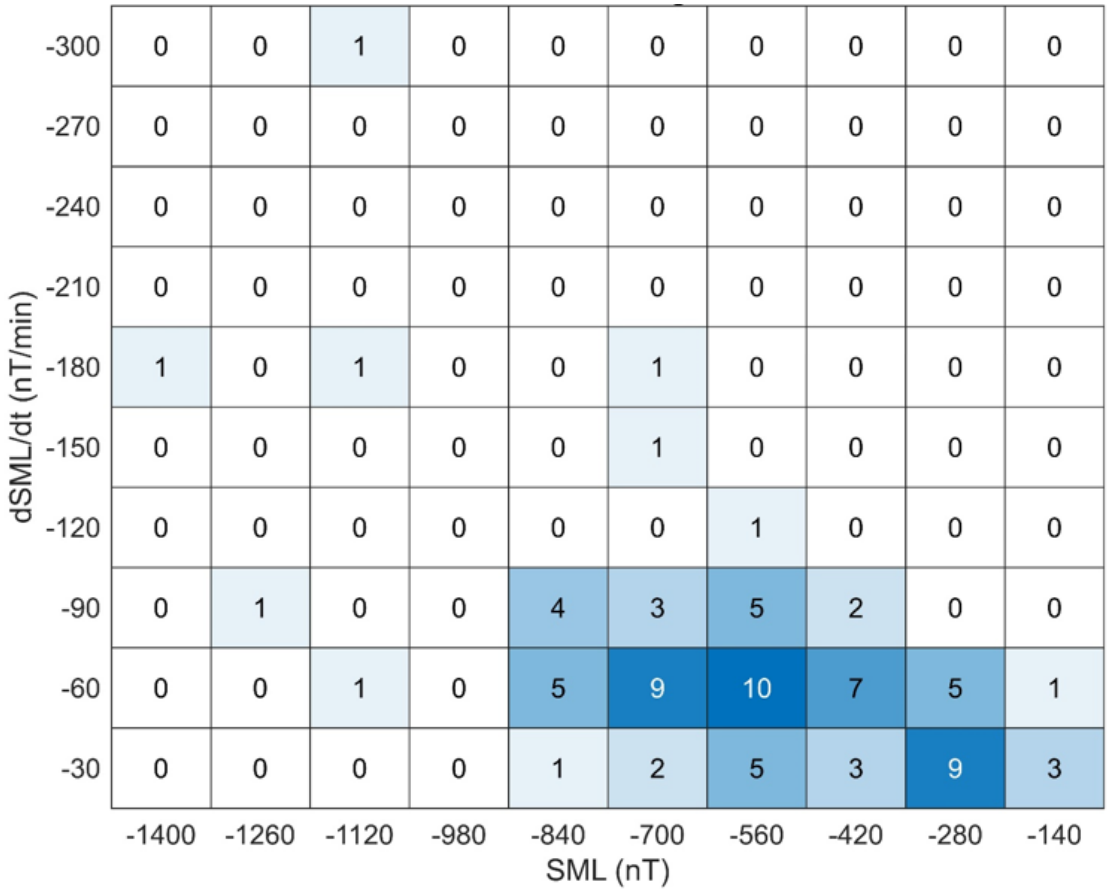

Figure 8. Heatmap analysis for the SML index and its time derivative (dSML/dt) surrounding substorm onsets.

3.3 Chapter Summary

While SuperMAG and THEMIS are not directly integrated or part of the same project, the data, and research from THEMIS and other satellite missions contribute to the broader knowledge of space weather conditions that SuperMAG and other ground-based networks monitor and analyze. The link between SuperMAG and THEMIS data lies in their complementary nature. SuperMAG data in conjunction with THEMIS data is used to gain a more comprehensive view of geomagnetic activity. THEMIS data offer detailed measurements within the magnetosphere, and SuperMAG data provides a global perspective of geomagnetic disturbances. Combining these datasets can lead to a better understanding of how global and local phenomena are connected and can help improve space weather forecasting and research in geomagnetic physics.

CHAPTER IV

SUBSTORM ONSET ANALYSIS USING WINDMI MODEL

4.1 WINDMI Model

Multi-scale modeling techniques were developed because of the complexity and diversity of the physical processes that occur during storms and substorms. The analysis of plasma flow and overall behavior of the magnetosphere-ionosphere system is carried out by Magnetohydrodynamics (MHD) simulations and low-order models.

MHD simulations divide a certain region into small grid cells and apply the full set of ideal plasma fluid equations to every cell (Lyon et al., 2004; Zhang et al., 2019). These methods attempt to analyze the plasma flows and the propagation of disturbances within the magnetosphere as accurately as possible and with high spatial and temporal resolution. Low-order models analyze the global or overall behavior of the magnetosphere-ionosphere system by reducing or combining the dynamics of various sections to simulate the interaction between key energy components.

An example of a low-order physics model is the WINDMI model (Horton et al., 1998; Spencer et al., 2007). The importance of analyzing the global or overall behavior of the magnetosphere-ionosphere system by reducing or combining the dynamics of various sections to simulate the interaction between key energy components while being fast and computationally inexpensive cannot be over-emphasized. The plasma physics-based

WINDMI model uses the solar wind dynamo voltage, Vsw, generated by a particular solar wind-magnetosphere coupling function to drive eight ordinary differential equations describing the transfer of power through the geomagnetic tail, the ionosphere, and the ring current.

The nonlinear equations of the model trace the flow of electromagnetic and mechanical energy through eight pairs of transfer terms. The remaining terms describe the loss of energy from the magnetosphere-ionosphere system through plasma injection, ionospheric losses, and ring current energy losses. The equations are derived from volume integrals of the plasma momentum and energy equations over the associated regions of the magnetosphere (Ebihara et al., 2019).

Equation (9) to (17) represent the equations of the model and the resultant circuit of the model is shown in Figure 9.

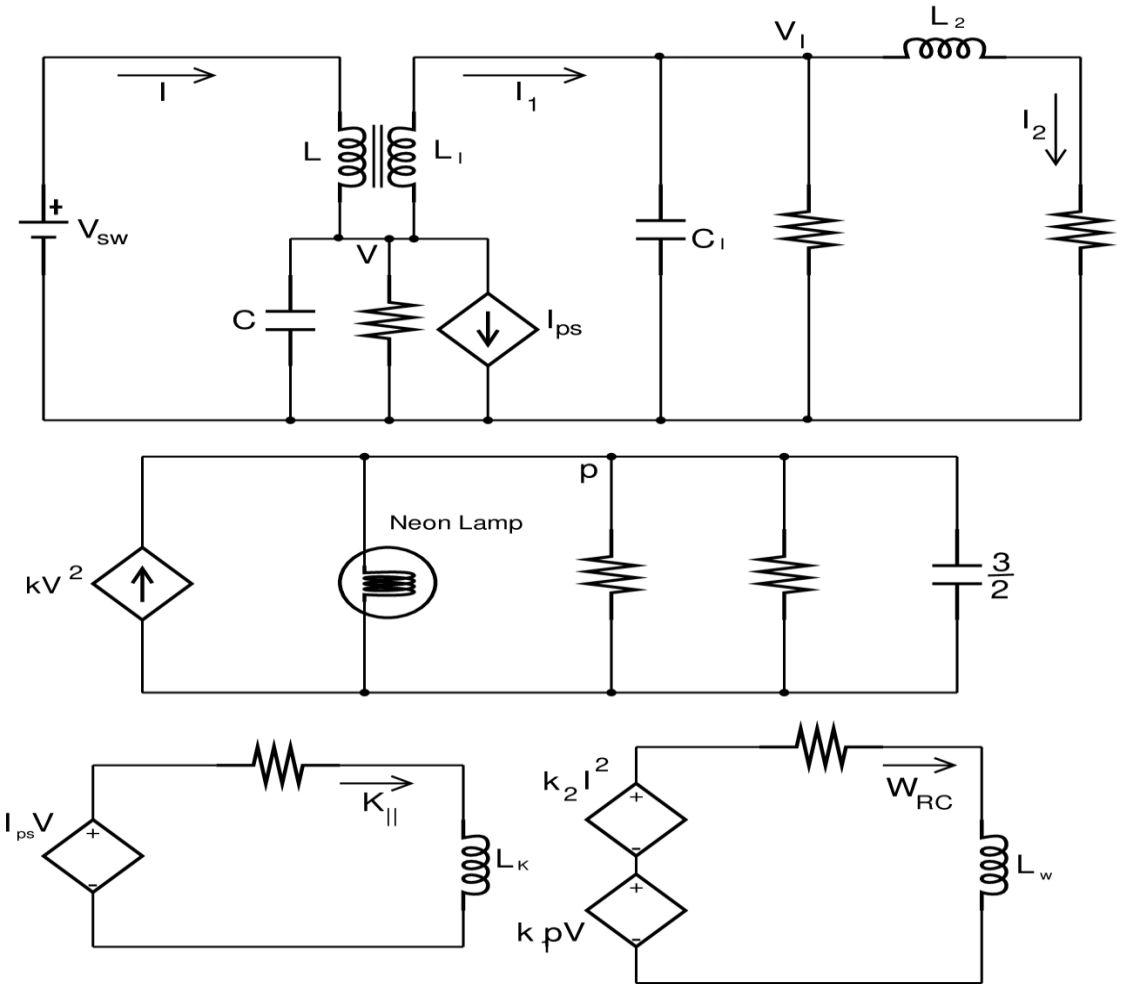

Figure 9. Equivalent circuit for the WINDMI model.

Figure 9 together with the set of nonlinear equations provides an understanding of the physical architecture of the WINDMI model. However, this is just one aspect of the model, as the input into the WINDMI model is a voltage that is proportional to a combination of solar wind parameters measured at L1 by the ACE satellite. In the differential equations, the coefficients are physical parameters of the magnetosphere-

ionosphere system, and the quantities L, C, L_1, C_1 and I are the magnetospheric and ionospheric inductances, capacitances, and conductance, respectively.

These parameters include the solar wind velocity (Vsw), the Interplanetary Magnetic Field (IMF) components (Bx, By, Bz), and the solar wind proton density (Np), measured in Geocentric Solar Magnetospheric (GSM) coordinates. To account for the propagation of the solar wind to the nose of the magnetosphere at 10 Earth radii (RE), these input parameters are time-delayed, as described in (Spencer et al., 2007). The logical architecture of the model encompasses the following steps.

The ACE data, as an input to the model, can undergo preprocessing to eliminate redundancy and correct flawed data using the K-nearest neighbor method. The presence of flawed data can significantly affect the model's efficiency.

The model operates in two modes based on the responses from the WINDMI model's circuitry.

1. Natural Response (Without Trigger). This mode occurs when the WINDMI circuit is open, meaning there is no voltage source ($V_{sw} = 0$). In this mode, the output is influenced by variations in the values of L and C. The circuit resembles an RLC circuit in parallel, with non-linear terms removed. Changes in L and C alter the circuit's oscillation behavior. The solar wind voltage source serves as an ideal power supply that controls the speed of the solar wind. The circuit in Figure 9 can be modified to generate a non-triggered output, allowing various parameters to deviate from their nominal values to produce an output for comparison with the SuperMAG AL and other indices.
2. Forced Response (With Trigger). The forced response occurs when the circuit is closed by adding a voltage source to power it. This compels currents to flow and limits the

impact of the circuit parameters. Adjusting the values of L and C enables the generation of triggered outputs. In this context, L represents the inductance and symbolizes the tail lobe of the magnetosphere.

The objective of this research is to establish the functional dependencies of each parameter within the model on various indices, measurements, and solar wind conditions. Our current investigations have revealed some initial dependencies, which are listed in column 4 of each table. These parameters may exhibit dependencies on factors such as solar wind velocity (V_{sw}), solar wind density (N_{sw}), Interplanetary Magnetic Field (IMF), plasma sheet density (N_{cps}), and others. It is essential to note that the dependencies provided in the tables are our initial expected relationships, and further dependencies may exist. Among the parameters that influence the behavior of the model during geomagnetic storms and impact the prediction of the D_{st} index are the geotail geometrical factor (_I) and the parameters described in the last two equations of the WINDMI model (equations 7 and 8). While this does not negate the significance of other factors, it suggests that the buildup and recovery rates of the ring current during prolonged geomagnetic storms are more dependent on these parameters at present. It is well-documented that the ring current decay rate (rc) is influenced by the solar wind electric field and dynamic pressure (Spencer et al., 2009). It is important to establish the robustness of the model to variations in Inductance and Capacitance because they represent the driving forces of magnetospheric activities. L is the magnetotail current and C is the inertia of particle collision.

Table 6. Nominal WINDMI parameters estimated based on physical characteristics of the nightside magnetosphere.

P	Nominal	Description	Dependencies
L	90 H	Inductance of the lobe cavity surrounded by the geotail current $I(t)$. The nominal value is $L = \mu_0 A_\ell / L_x^{\text{eff}}$ in Henries where A_ℓ is the lobe area and L_x^{eff} the effective length of the geotail solenoid.	v_{sw}, B^{IMF}
M	1 H	The mutual inductance between the nightside region 1 current loop I_1 and the geotail current loop I.	To research
C	50000 F	Capacitance of the central plasma sheet in Farads. The nominal value is $C = \rho_m L_x L_z / (B^2 L_y)$ where ρ_m is the mass density in kg/m^3, $L_x L_z$ is the meridional area of the plasma sheet, L_y the dawn-to-dusk width of the central plasma sheet and B the magnetic field on the equatorial plane.	N_{cps}, O^+/H^+
Σ	8 S	Large gyroradius ρ_i plasma sheet conductance from the quasineutral layer of height $(L_z \rho_i)^{1/2}$ about the equatorial sheet. The nominal value is $\Sigma = 0.1(n_e/B_n)(\rho_i/L_z)^{1/2}$.	N_{sw}, E_{sw}
Ω_{cps}	$2.6\times10^{24} m^3$	Volume of the central plasma sheet that supports mean pressure $p(t)$, initial estimate is $10^4 R_E^3$.	v_{sw}, B^{IMF}, N_{sw}
u_0	$4 \times 10^{-9} m^{-1} kg^{-1/2}$	Heat flux limit parameter for parallel thermal flux on open magnetic field lines $q_\parallel = const \times v_\parallel p = u_0 (K_\parallel)^{1/2} p$. The mean parallel flow velocity is $(K_\parallel/(\rho_m \Omega_{cps}))^{1/2}$.	To research
I_c	1.78×10^7 A	The critical current above which unloading occurs.	To research
α	8×10^{11}	The geotail current driven by the plasma pressure p confined in the central plasma sheet. Pressure balance between the lobe and the central plasma sheet gives $B_\ell^2/2\mu_0 = p$ with $2L_x B_\ell = \mu_0 I_{ps}$. This defines the coefficient α in $I_{ps} = \alpha p^{1/2}$ to be approximately $\alpha = 2.8 L_x / \mu_0^{1/2}$.	To research
τ_E	30 min	Characteristic time of thermal energy loss through earthward and tailward boundary of plasma sheet.	To research
L_1	20 H	The self-inductance of the wedge current or the nightside region 1 current loop $I_1(t)$	To research
C_I	800 F	The capacitance of the nightside region 1 plasma current loop.	To research
Σ_I	3 mho	The ionospheric Pedersen conductance of the westward electrojet current closing the I_1 current loop in the auroral (altitude $\sim$ 100 km, 68°) zone ionosphere.	N_{cps}, $F_{10.7}$, E_{sw}

Table 6 (continued).

R_{prc}	0.1 ohm	The resistance of the partial ring current.	To research
τ_{rc}	12 hrs	The decay time for the ring current energy.	$E_s w$, $P_{sw}^{1/6}$
L_2	8 H	The inductance of the region 2 current.	To research
R_{A2}	0.3 ohm	Resistance of the region 2 footprint in the Auroral Region.	To research
B_{tr}	5×10^{-9} T	The magnetic field in the transition region.	To research
A_{eff}	8.14×10^{13} m^2	The average effective area presented to the geotail plasma for plasma entry into the inner magnetosphere, estimated to be $2R_E^2$.	To research
L_y	3.2×10^7 m	The effective width of the Alfven layer aperture, estimated to be $5R_E$.	v_{sw}, B^{IMF}, N_{sw}
ΔI	1.25×10^5 A	The rate of turn-on of the unloading function.	To research
α_I	4.3	Geotail current contribution to Dst index	v_{sw}, B^{IMF}, N_{sw}

Table 6 shows model parameters and how they influence the model. These parameters will be adapted to time-dependent variations in response to solar wind and magnetospheric conditions

The robustness of the circuit to variations of these parameters is not of primary importance because they are not the driving forces of magnetospheric activities.

4.2 WINDMI Model Output for the Selected Events

One of the primary objectives of this research project is to investigate the relationship between model data and observed data in the field of geomagnetic activity. Specifically, this research aims to use the WINDMI model to establish correspondence between the model's output (I1) which represents field-aligned current, and the widely recognized Super Magnetospheric Lobe (SML) index. The SML index serves as a

quantitative measure of geomagnetic activity and is a crucial indicator in space physics and magnetospheric research.

The dependence of the output on time is also compared with the gradient of the SML. Find below the plots showing the relationship between 11 and SML for the selected events on a 24-hour scale. The selected events include.

4.2.1 January 07, 2000

Panel (a) displays the half-wave rectified solar wind input propagated forward by one hour, serving as an input to the WINDMI model. Panels (b) and (c) illustrate the field aligned current I1 and its slope in black lines. Panel (d) presents the SML indices. In Panels (b), (c), and (d), the colored vertical dotted lines indicate substorm onsets detected at those times by various techniques. The colors of the onsets represent the number of techniques that coincidentally detected the specific substorm (purple, blue, green, and red correspond to four, three, two, and one method(s) detecting the onsets). The labels in Panel (d) are abbreviations of the authors who invented the techniques. 'Fo' for (Forsyth et al., 2015) 'Fr' for (Frey et al., 2004), ‘Li’ for (Newell et al., 2010)), 'Ne' for (Newell & Gjerloev, 2011), and 'Oh' for (Ohtani & Gjerloev, 2020).

The SML plots show that even when the criteria are different, there are still crossings. Determining the correlation between SML and I1 may help identify the range, if not the exact magnitude, at which onset occurs. This can help explain why the onset timings for the various criteria varied and sometimes intersected.

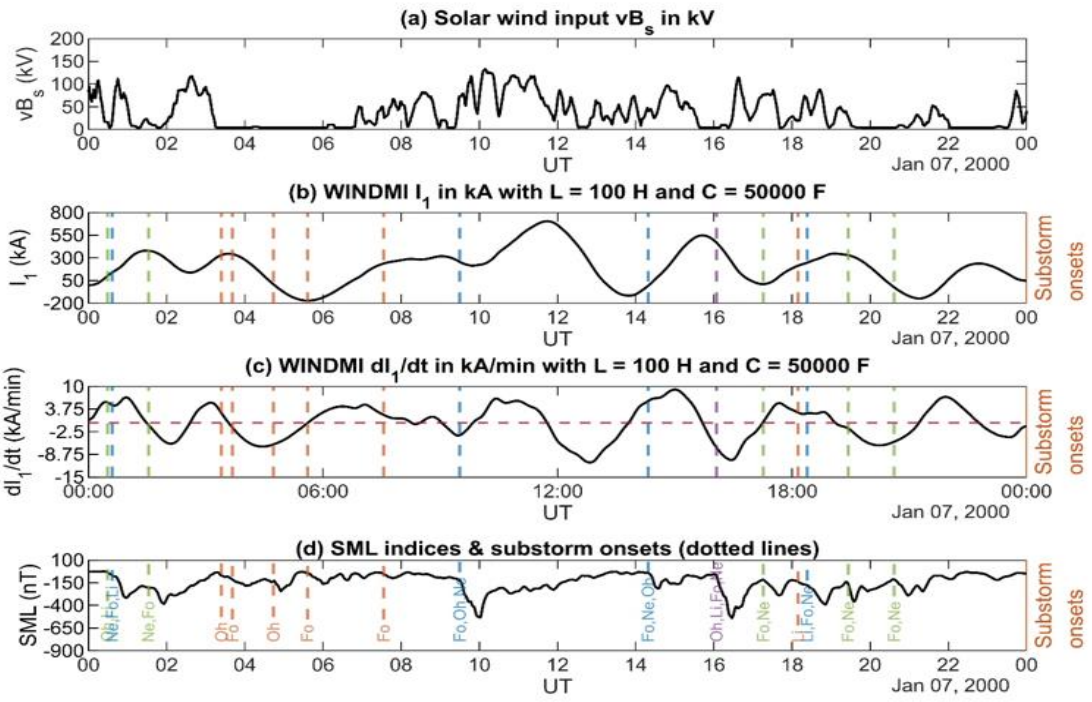

Figure 10. WINDMI outputs for January 07, 2000, with nominal values of L and C (L = 100H, C = 5000F).

4.2.2 April 24, 2003

Panel (a) displays the half-wave rectified solar wind input propagated forward by one hour, serving as an input to the WINDMI model. Panels (b) and (c) illustrate the field aligned current I1 and its slope in black lines. Panel (d) presents the SML indices. In Panels (b), (c), and (d), the colored vertical dotted lines indicate substorm onsets detected at those times by various techniques. The colors of the onsets represent the number of techniques that coincidentally detected the specific substorm (purple, blue, green, and red correspond to four, three, two, and one method(s) detecting the onsets). The labels in Panel (d) are abbreviations of the authors who invented the techniques ‘Fo' (Forsyth et al., 2015) 'Fr' (Frey et al., 2004), 'Li' (Newell et al., 2010), 'Ne' for (Newell & Gjerloev,

2011), and 'Oh' for (Ohtani & Gjerloev, 2020). Figure 10 shows the WINDMI outputs and their dependence on time for January 7, 2000, at nominal values of L and C (L = 100 H, C = 50000 F) and SML plot referencing the geomagnetic activity for the day.

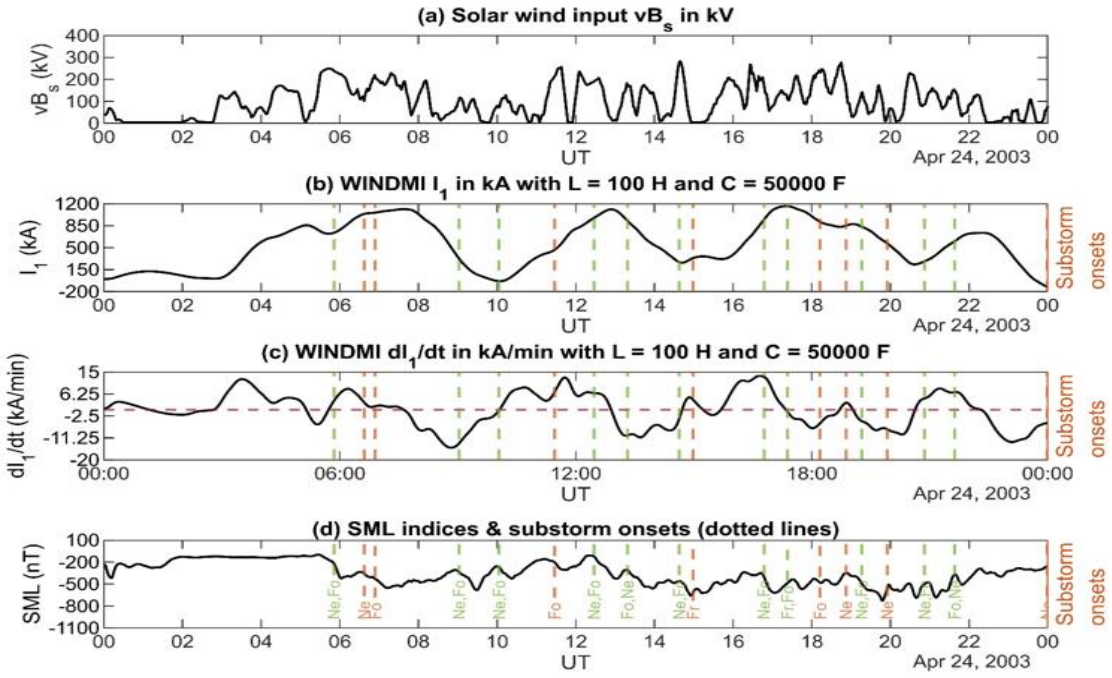

Figure 11. WINDMI outputs for April 24, 2003, with nominal values of L and C (L = 100H, C = 5000F).

4.2.3 March 09, 2008

Panel (a) displays the half-wave rectified solar wind input propagated forward by one hour, serving as an input to the WINDMI model. Panels (b) and (c) illustrate the field aligned current I1 and its slope in black lines. Panel (d) presents the SML indices. In Panels (b), (c), and (d), the colored vertical dotted lines indicate substorm onsets detected at those times by various techniques. The colors of the onsets represent the number of

techniques that coincidentally detected the specific substorm (purple, blue, green, and red correspond to four, three, two, and one method(s) detecting the onsets). The labels in Panel (d) are abbreviations of the authors who invented the techniques.

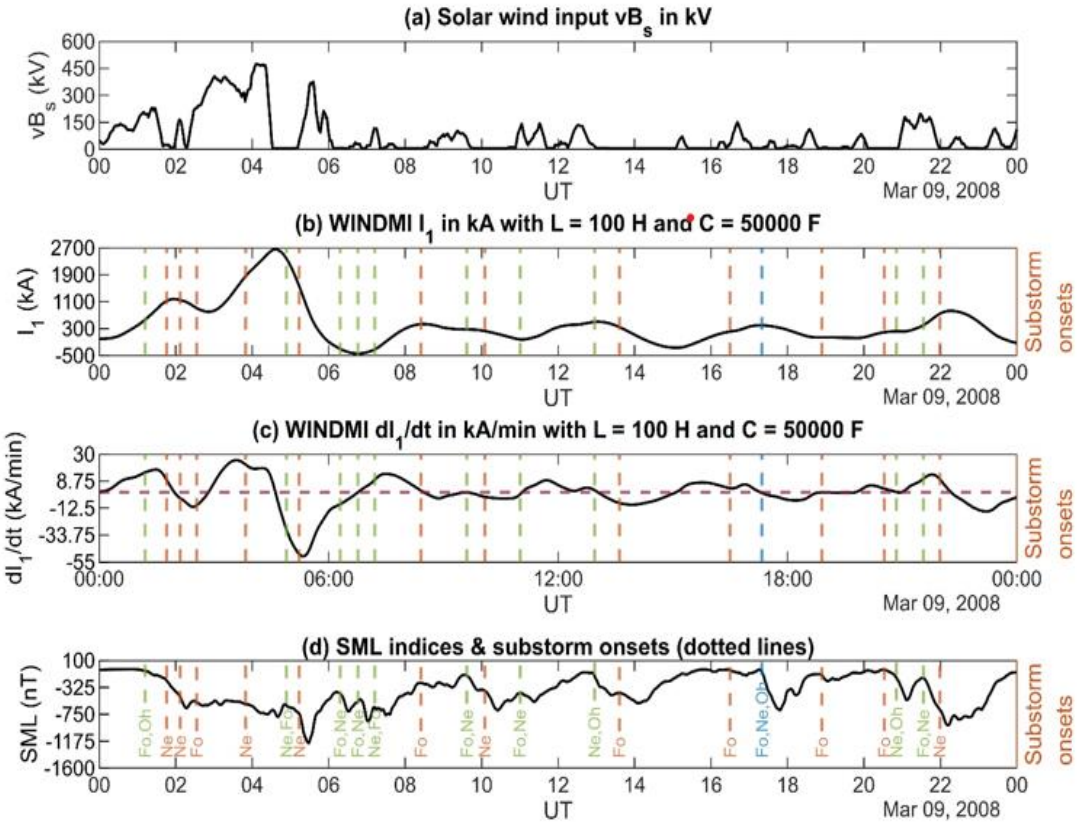

Figure 12. WINDMI outputs for March 09, 2008, with nominal values of L and C (L = 100H, C = 5000F).

4.2.4 April 26, 2013

Panel (a) displays the half-wave rectified solar wind input propagated forward by one hour, serving as an input to the WINDMI model. Panels (b) and (c) illustrate the field aligned current I1 and its slope in black lines. Panel (d) presents the SML indices. In

Panels (b), (c), and (d), the colored vertical dotted lines indicate substorm onsets detected at those times by various techniques. The colors of the onsets represent the number of techniques that coincidentally detected the specific substorm (purple, blue, green, and red correspond to four, three, two, and one method(s) detecting the onsets).

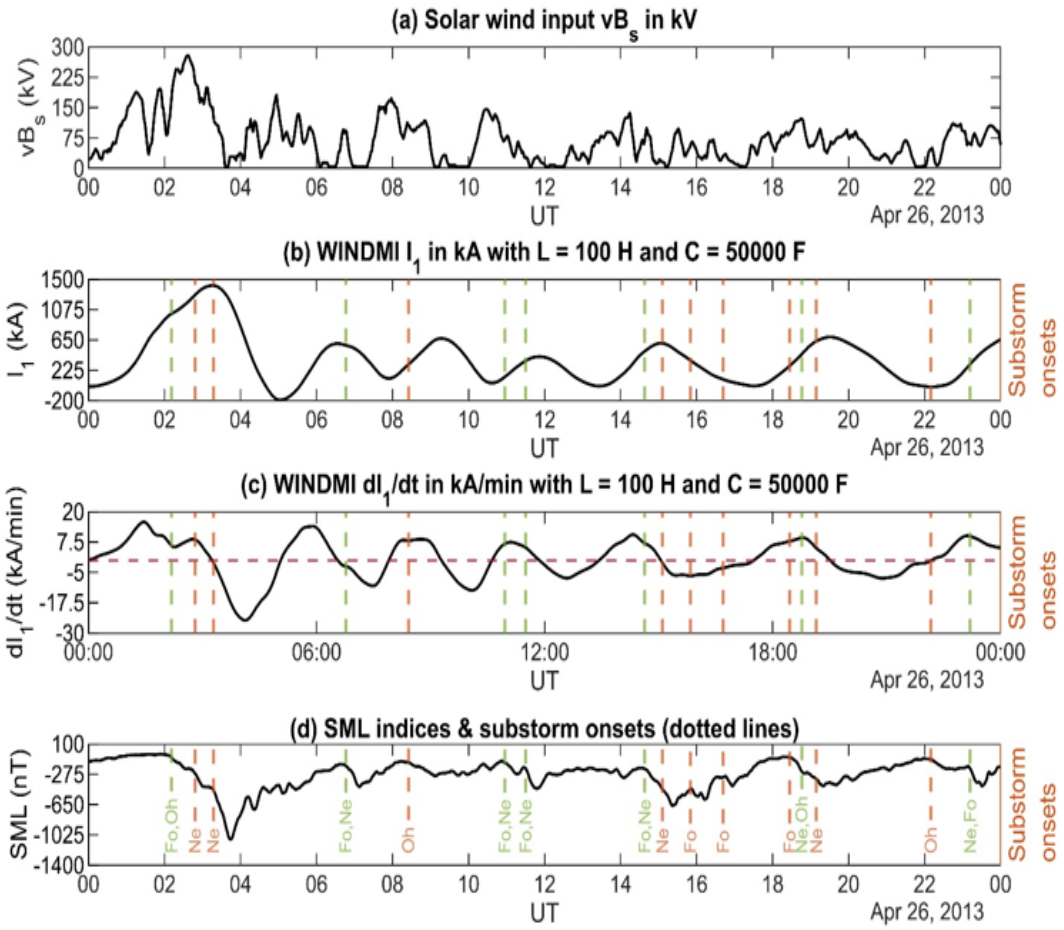

Figure 13. WINDMI outputs for April 26, 2013, with nominal values of L and C (L = 100H, C = 5000F).

4.2.5 August 09, 2016

Panel (a) displays the half-wave rectified solar wind input propagated forward by one hour, serving as an input to the WINDMI model. Panels (b) and (c) illustrate the field aligned current I1 and its slope in black lines. Panel (d) presents the SML indices. In Panels (b), (c), and (d), the colored vertical dotted lines indicate substorm onsets detected at those times by various techniques. The colors of the onsets represent the number of techniques that coincidentally detected the specific substorm (purple, blue, green, and red correspond to four, three, two, and one method(s) detecting the onsets).

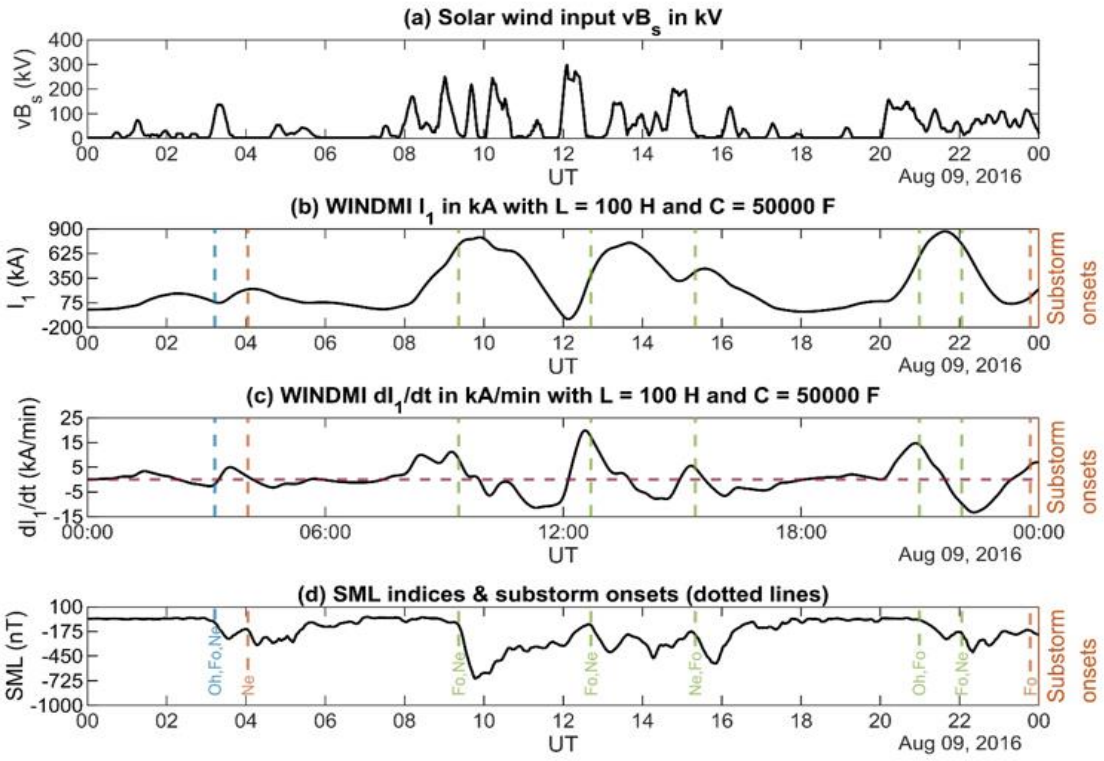

Figure 14. WINDMI outputs for August 09, 2016, with nominal values of L and C (L = 100H, C = 5000F).

Having generated the output for the selected dates, a general assumption to show the relationship between the WINDMI field-aligned current and SML index is important to generate a ground truth. The relationship between I1 and its slope is proportional to the true value relationship between SML and its rate of change with respect to time. To determine the rate of change of I1 with time, a peak point is determined, the peak point is denoted in blue and red. The red corresponds to maximum values within which there are substorm onsets predicted by existing criteria while the blue represents peak point detected only by WINDMI. WINDMI output with peak point denoted is shown below.

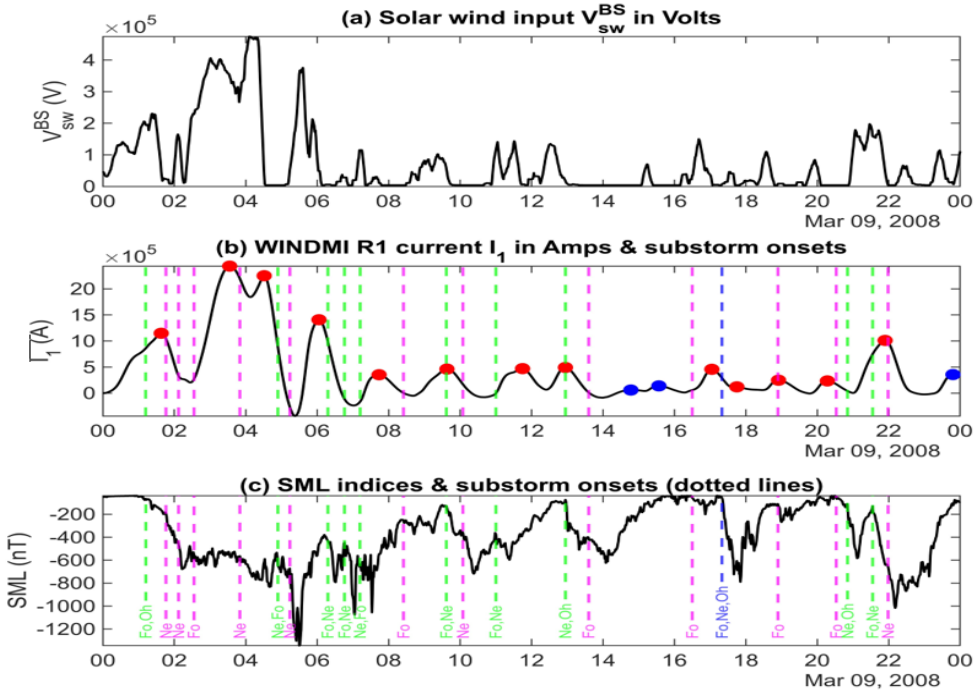

Figure 15. WINDMI output plots with peak period denoting maximum point for calculating the rate of change of current with time

The peak point is used to calculate the gradient of the field-aligned current. The relationship between dI1/dt and field aligned current I1 is shown in the heatmap below.

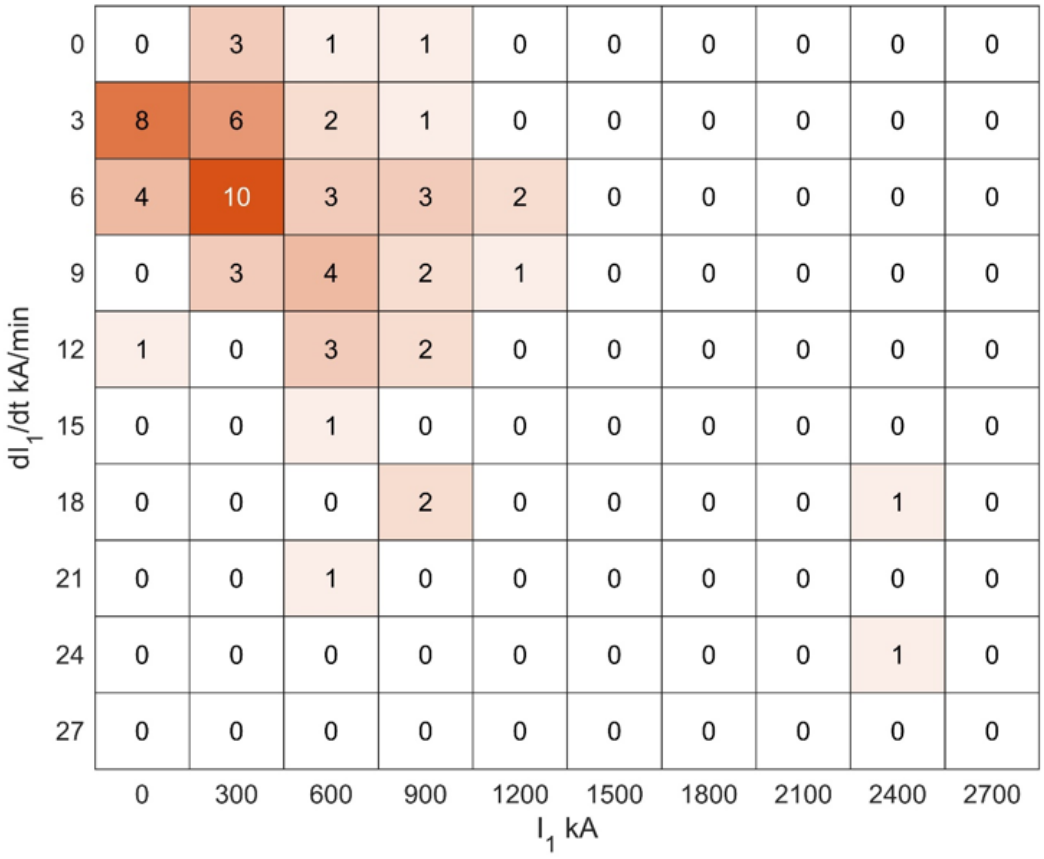

Figure 16. Heatmap analysis for the maximum field aligned current I1 and dI1/dt surrounding substorm onsets for nominal values of L and C.

In Figure 16, I1 is divided into 10 bins, ranging from 0 to 3000 kA. The labels associated with the bins represent the first value of each bin, with each bin having a range of 300 kA. For dI1/dt, the number of bins is the same, covering a total range of 0 to 30 kA/min. Each bin for dI1/dt spans 3 kA/min. The heatmaps illustrate the counts of

substorm onsets for the corresponding bins. I1 and dI1/dt are calculated by taking the maximum values of I1 and dI1/dt within a period spanning 30 minutes before and 30 minutes after the detected substorm onsets. If substorms occur within the 30-minute boundary on either side, they are considered as the boundaries for the time. The relationship between the gradient of WINDMI output and the SML index gradient is shown in the heatmap below.

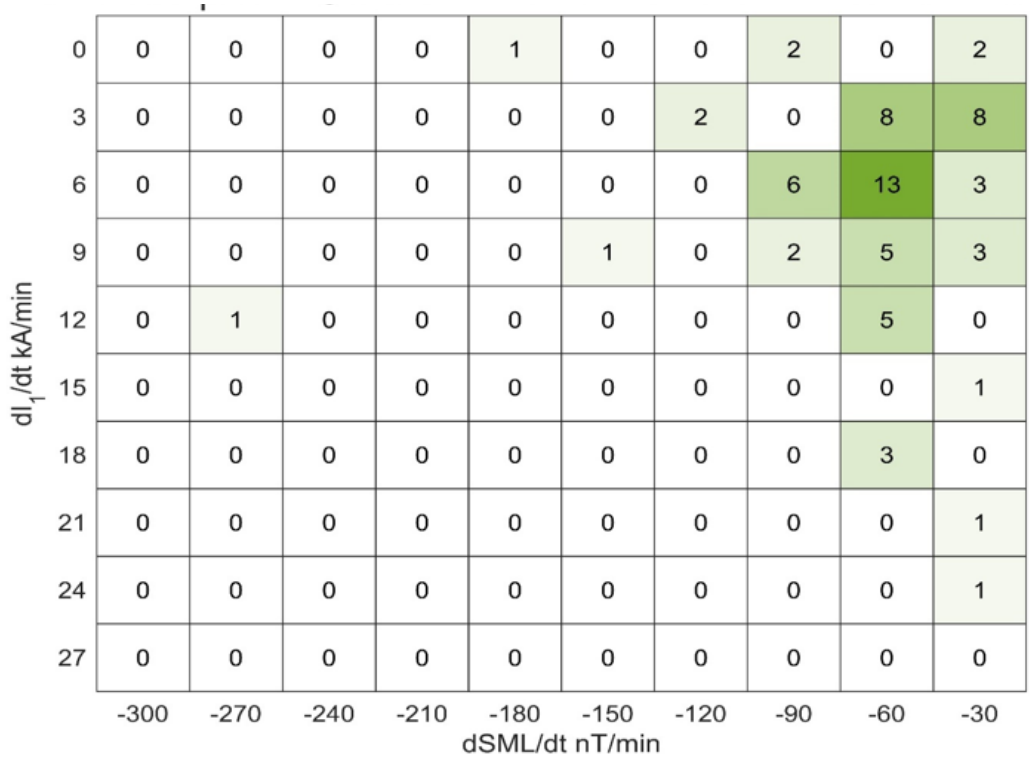

Figure 17. Heatmap analysis for the maximum dI1/dt and dSML/dt surrounding substorm onsets.

The labels associated with the bins in Figure 17 represent the first value of each bin, with each bin having a range of 3 kA/min. For dSML/dt, the number of bins is the same, covering a total range of -300 to 0 nT/min. Each bin for dSML/dt spans 30 nT/min. The heatmaps illustrate the counts of substorm onsets for the corresponding bins.

For dSML/dt, the maximum values are determined from the onset of the substorm and extend to 30 minutes after the onset time. Since current (I) and magnetic field intensity (B) are intimately correlated, understanding how current varies with circuit parameter modification is necessary to comprehend the model's sensitivity. L and C variations are more important in the model which recreates the ‘store and release’ geomagnetic phenomena. Inductors store electrical energy in the form of a magnetic field when current flows through it. It resists changes in the current, introducing inductive reactance in AC circuits. WINDMI plots for varying parameter conditions are shown below.

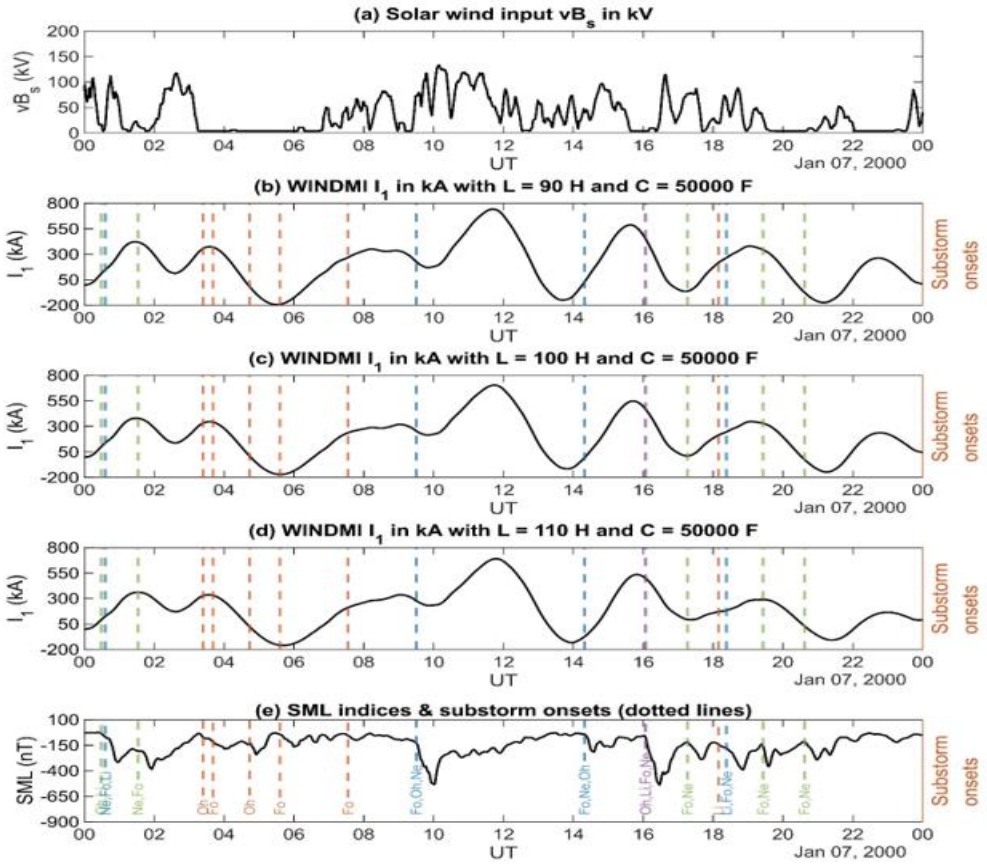

Figure 18. WINDMI model outputs with varying L (+-10% deviation from nominal values of L = 100 H) for January 7, 2000.

Panel (a) displays the solar wind rectified input used as the model's input. Panels (b), (c), and (d) show the currents I1 with L values of 90, 100, and 110 H, respectively. Panel (e) presents the SML indices throughout the day.

Figure 18 illustrates the changes in the magnitudes and trends of I1 with variations in L. The variation is a +- 10% deviation of L from its nominal value while keeping C constant at nominal. The plots don't show much difference in the variations. The model is robust enough not to show sensitivity for a +- 10% change in inductance

value. The plots below represent the model output to a 10% change in capacitance keeping inductance constant at nominal.

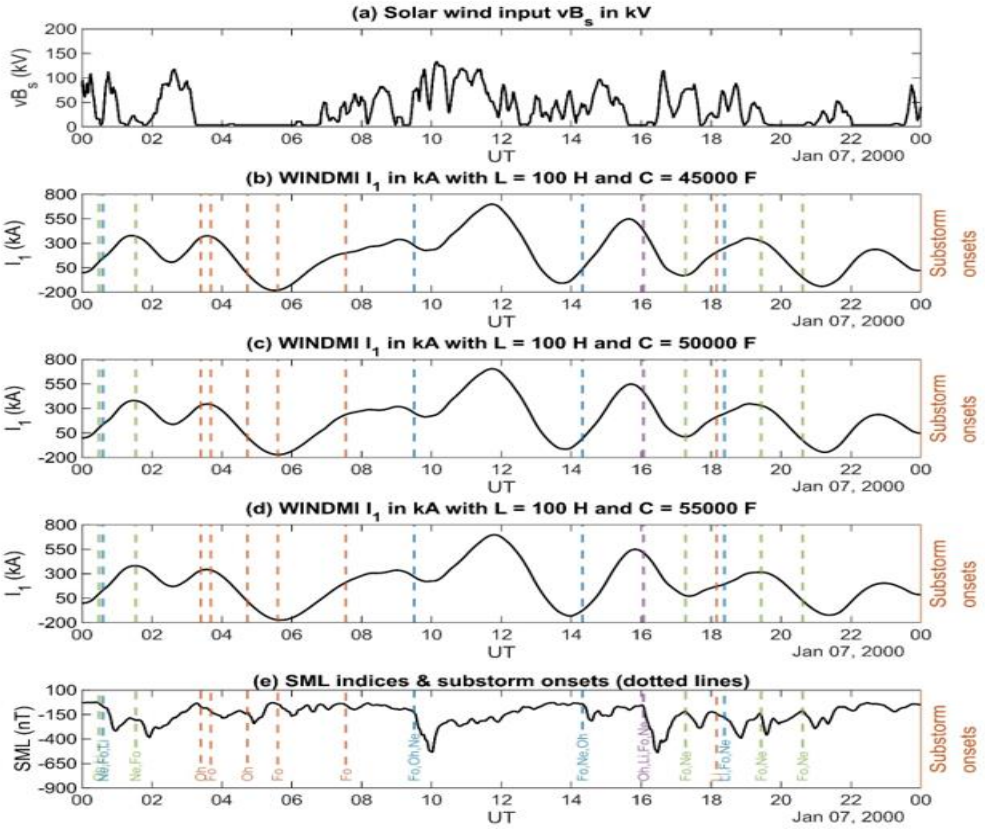

Figure 19. WINDMI model outputs with varying C (+-10% deviation from nominal values of L = 100 H) on January 7, 2000.

Panel (a) displays the solar wind rectified input used as the model's input. Panels (b), (c), and (d) show the currents I1 with C values of 45000, 50000, and 55000 F, respectively. Panel (e) presents the SML indices throughout the day.

It can be seen from Figure 19 that altering the capacitance at the nominal value of L does not have a noticeable change in the output of the model. The orientation of the current

with respect to time remains the same but the magnitude changes. A higher value of C reflects a reduction in current as well as a shift in resonant frequency to lower values. Figure 20 explains the ripple effect of a 10% deviation of L and C from nominal value.

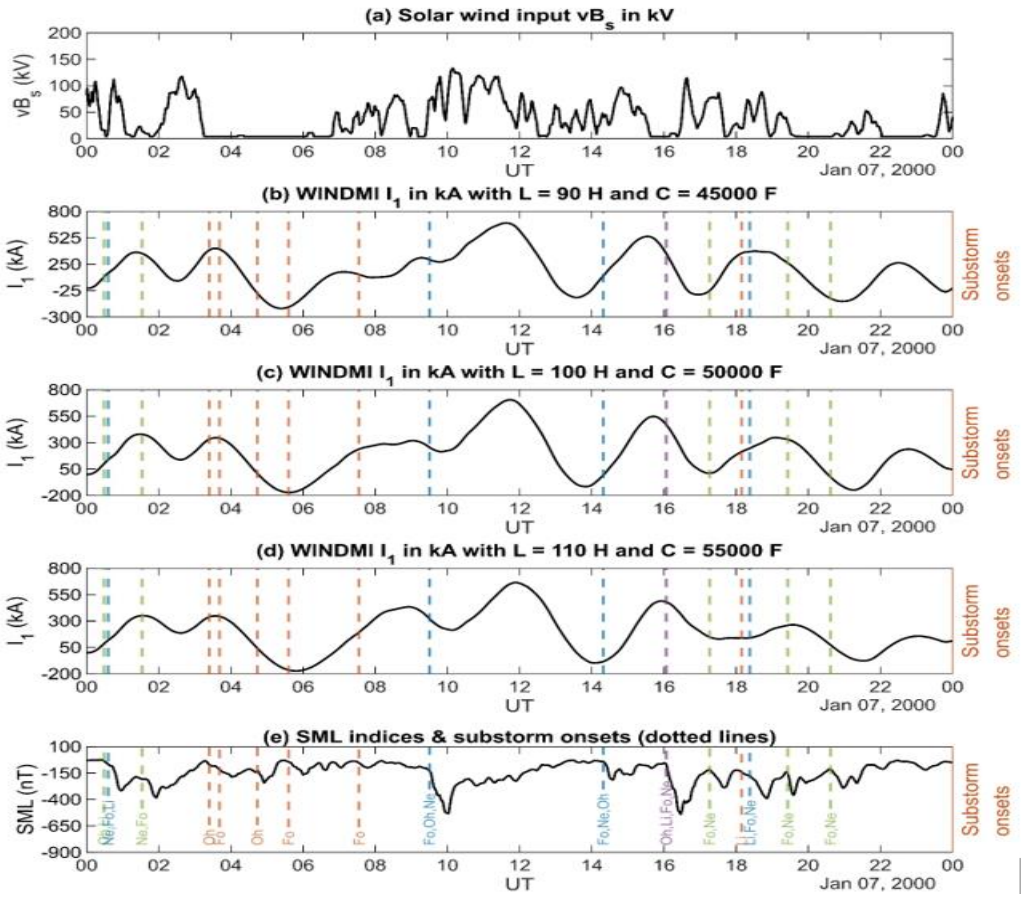

Figure 20. WINDMI model outputs with varying both L and C (+-10% deviation from their respective nominal values) for January 7, 2000.

The blue line represents the slope (rate of change of current with time) which is compared with dsml/dt to establish an inference in this research. The same is repeated for the other selected events.

4.3 Chapter Summary

The number of onsets identified by WINDMI is less than or equal Number of onsets identified by the list. WINDMI could identify a minimum number of substorms but not necessarily all the events. The extent of variation that affects the model entirely defines the model sensitivity and this is a critical aspect of model assessment and performance evaluation.

The magnitude of the SML at onset times can explain why there are intersections even when the criteria are different.

CHAPTER V

STATISTICAL RELATIONSHIP BETWEEN SUPERMAG AND WINDMI OUTPUT

Several statistical approaches and data analysis methods were employed in determining the link between the SuperMAG (Super Magnetometer) data and WINDMI. To establish a statistical link, the output of the WINDMI model, which is a linear model showing how the Earth's magnetic field behaves under various circumstances is compared with the observational data from SuperMAG.

For a very long time, methods of identifying substorms focused on visual observation of abrupt increases in auroral brightness that resulted in the construction of an auroral arc and its motion towards the polar regions (Akasofu, 2004). These methods frequently relied on the time of the sudden brightness of the auroral arc (Maimaiti et al., 2019). This method was laborious and subjectively depended on the observer's judgment, the uncertainty in the results of these methods spurred the automation and quantitative methods of substorm onset determination.

During a substorm, the H component of the auroral electrojet index exhibits a sudden decrease during its expansion phase, returning to quiet levels during the recovery phase. Substorms are identified by analyzing the signature of substorms in the low

auroral electrojet (AL), where substorms were characterized by a sudden drop in the AL index during the expansion phase followed baseline during the recovery phase.

Newell and Gjerloev (2011) introduced the SML index, representing the minimum H value observed among all stations with transformed coordinates and baseline subtraction. Their automated baseline removal procedure effectively eliminated yearly and daily variations as well as contributions from the solar quiet day current system. They formulated rules based on the SML index, requiring a sharp drop in SML within 3 minutes after the onset of the substorm, with the SML value remaining less than an average of -100nT for the next 26 minutes.

The "SML" and "dSML/dt" parameters are used to describe and quantify geomagnetic disturbances and storm-level events. SML is calculated based on measurements of the horizontal components of the magnetic field (H) obtained from various SuperMAG magnetometer stations. SML (SuperMAG Local Index) is an index that quantifies the level of geomagnetic activity and disturbance at a specific time and location. It is typically expressed in nanoteslas (nT) and represents the deviation of the horizontal magnetic field from its quiet-time reference level.

SML provides a measure of how much the Earth's magnetic field is being perturbed by external factors, such as solar activity.

dSML/dt (Rate of Change of SuperMAG Local Index). The dSML/dt parameter is a derivative of the SuperMAG Local Index and measures the rate of change of

geomagnetic activity. It indicates how quickly the magnetic field is changing in response to external influences. dSML/dt is often expressed in nanoteslas per minute (nT/min). Positive values of dSML/dt indicate an increase in geomagnetic activity, while negative values suggest a decrease. It is a useful parameter for identifying sudden geomagnetic disturbances, such as the onset of geomagnetic storms. Both the SML and dSML/dt parameters are essential for monitoring and characterizing geomagnetic storm events and space weather. WINDMI model, although not a time-varying state-dependent model of the magnetosphere, has comparatively been able to replicate and make predictions of substorm onsets.

The current output and its gradient equivalents for the selected events are shown below. Heatmap visualizes relationships and patterns within data using color intensity to represent the value of data points. Heatmap of different variations represents the sensitivity of the field-aligned current to the respective variation of the model parameters.

Figure 21 shows the clustering of heatmaps for deviations from nominal values of L and C.

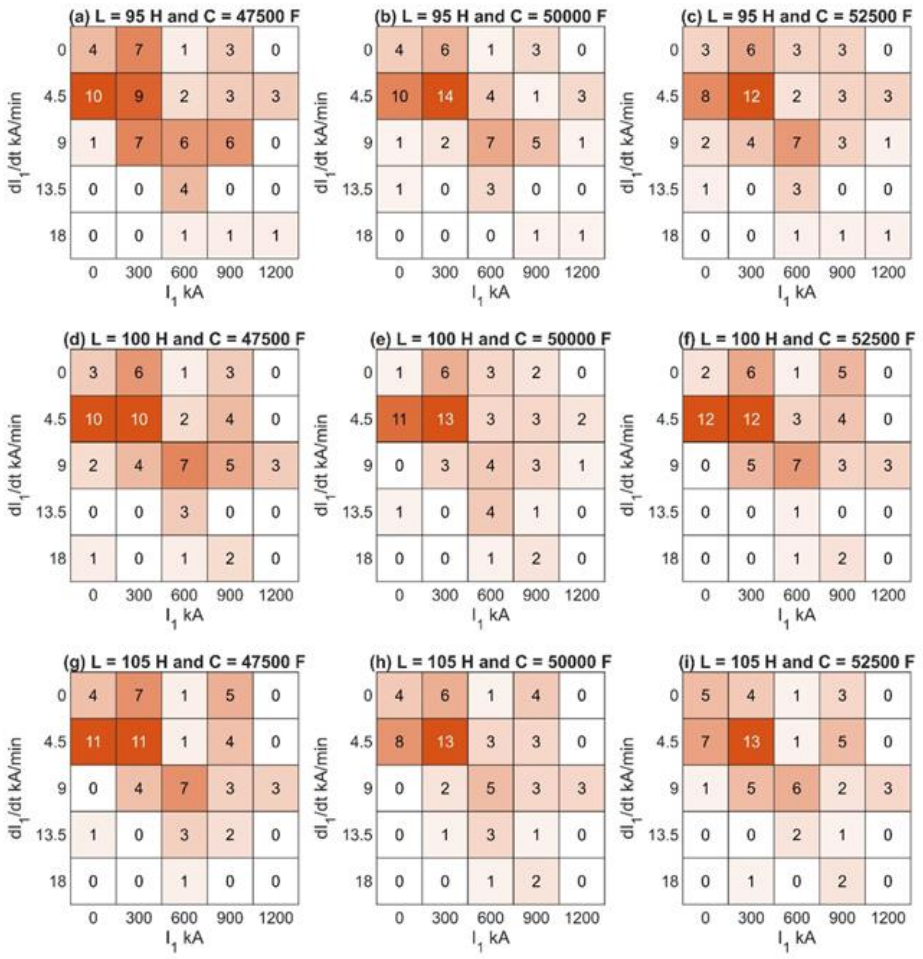

Figure 21. A cluster of heatmaps illustrating the variations in the values of I1 and dI1/dt resulting from 5% deviations in L and C from their nominal values.

Panel (e) displays a heatmap (with certain marginal values excluded to highlight the pattern change) of I1 and dI1/dt. The remaining panels depict heatmaps for different combinations of L and C values, with the top row panels (a, b, c) showing lower values of L (reduced by 5%), and the bottom row panels (g, h, i) displaying higher values of L (increased by 5%). Likewise, the left column panels (a, d, g) feature lower values of C (reduced by 5%), while the right column panels (c, f, i) exhibit higher values of C

(increased by 5%). The values of I1 and dI1/dt for a much higher deviation are shown in Figure 22.

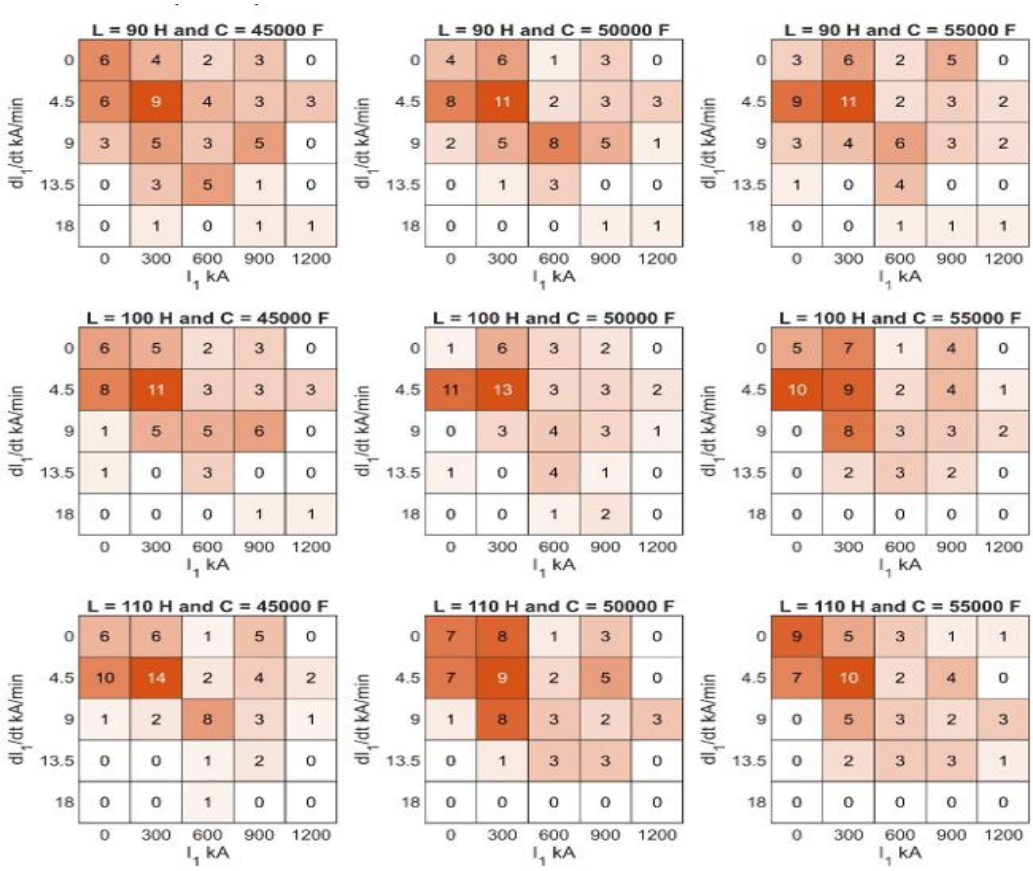

Figure 22. A cluster of heatmaps illustrating the variations in the values of I1 and dI1/dt resulting from 10% deviations in Inductance L and Capacitance C from their nominal values.

Figure 22 explains the effects of 10% variations in L and C values on field-aligned current and its gradient. The titles of each panel specify the corresponding L and C values. The figure demonstrates that substorm onset counts tend to cluster at I1 values

in the range of 300 to 600 kA and dI1/dt values in the range of 4.5 to 9 kA/min. These clustering tendencies diminish as L and C values deviate from their nominal values.

The figure illustrates that as L and C values deviate further from their nominal values, the previously observed clustering tendencies in substorm onset counts become further diminished. The relationship between the gradient of WINDMI output and SML index gradient also showed changes with deviation in L and C. This can be seen in Figure 23.

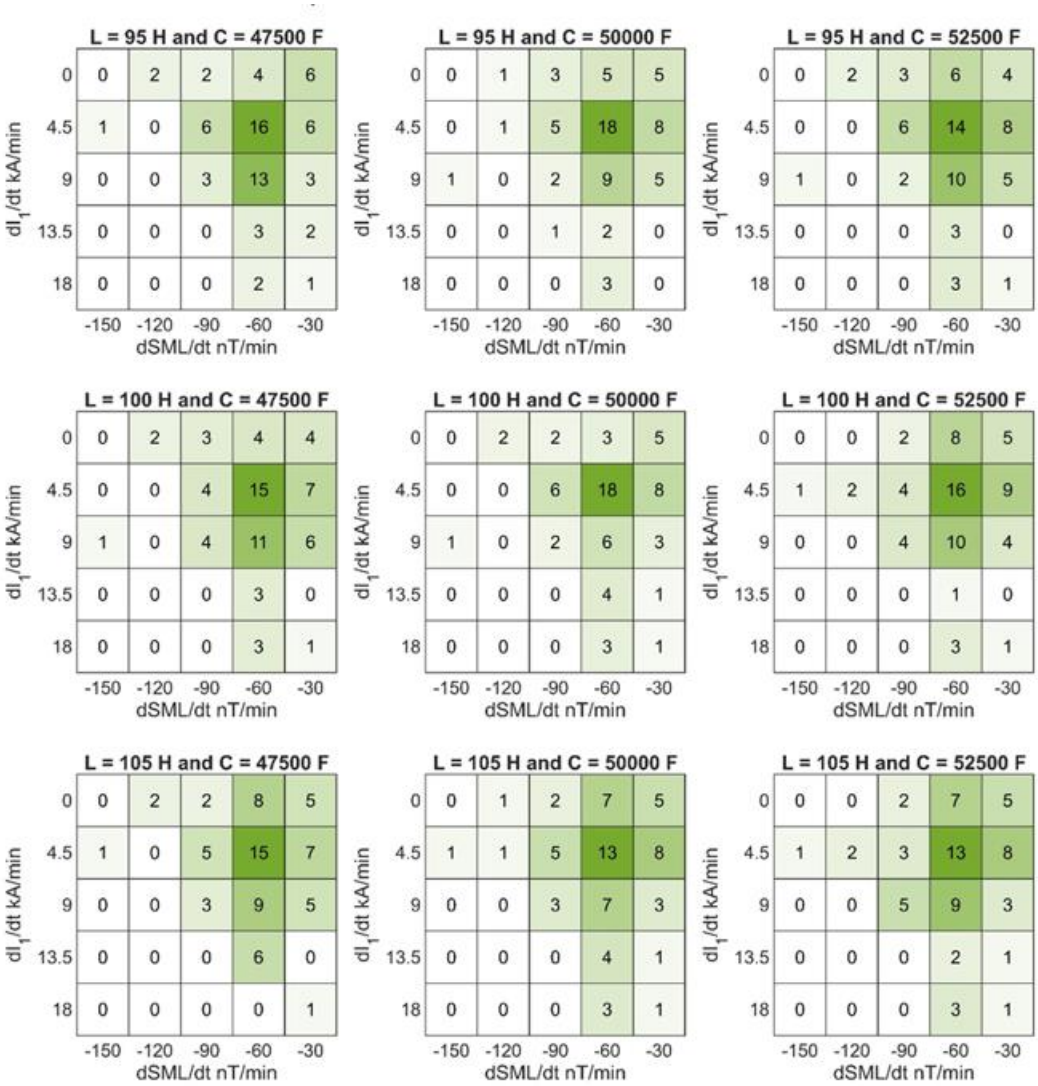

Figure 23. A cluster of heatmaps illustrating the variations in the values of dI1/dt and dSML/dt resulting from 5% deviations in L and C from their nominal values.

The heatmaps highlight how clustering tendencies evolve as L and C values deviate further from the nominal parameters. A plot showing the relationship between dSML/dt and dI1/dt for a 10% deviation of L and C from nominal values is shown below.

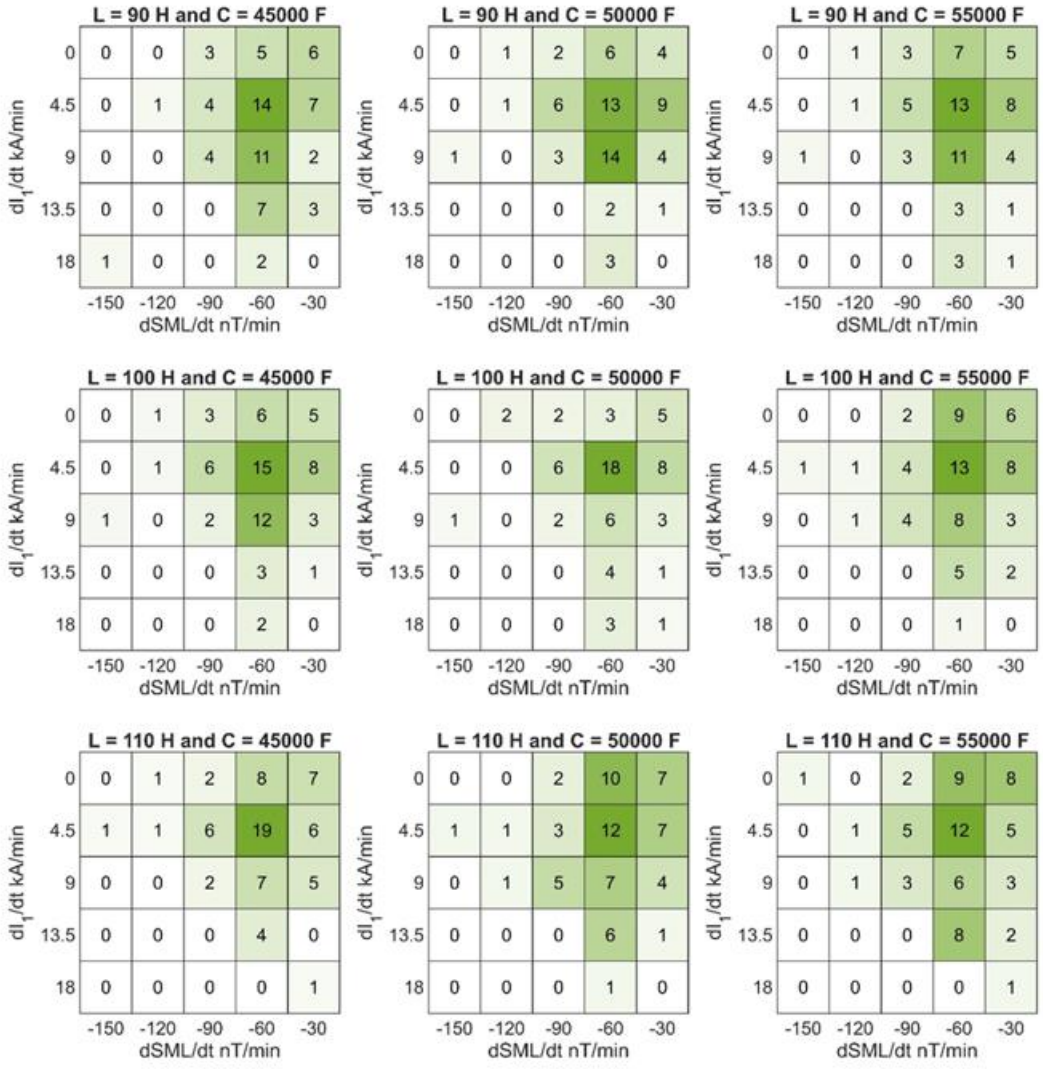

Figure 24. Plots showing the variations of dI1/dt and dSML/dt resulting from 10% deviations in Inductance and Capacitance from their nominal values.

The heatmaps demonstrate how substorm onset clustering tendencies change as inductance L and Capacitance C values deviate more significantly from their nominal values, providing further insights into the behavior of these parameters. The clustering change for a 20% deviation is shown below.

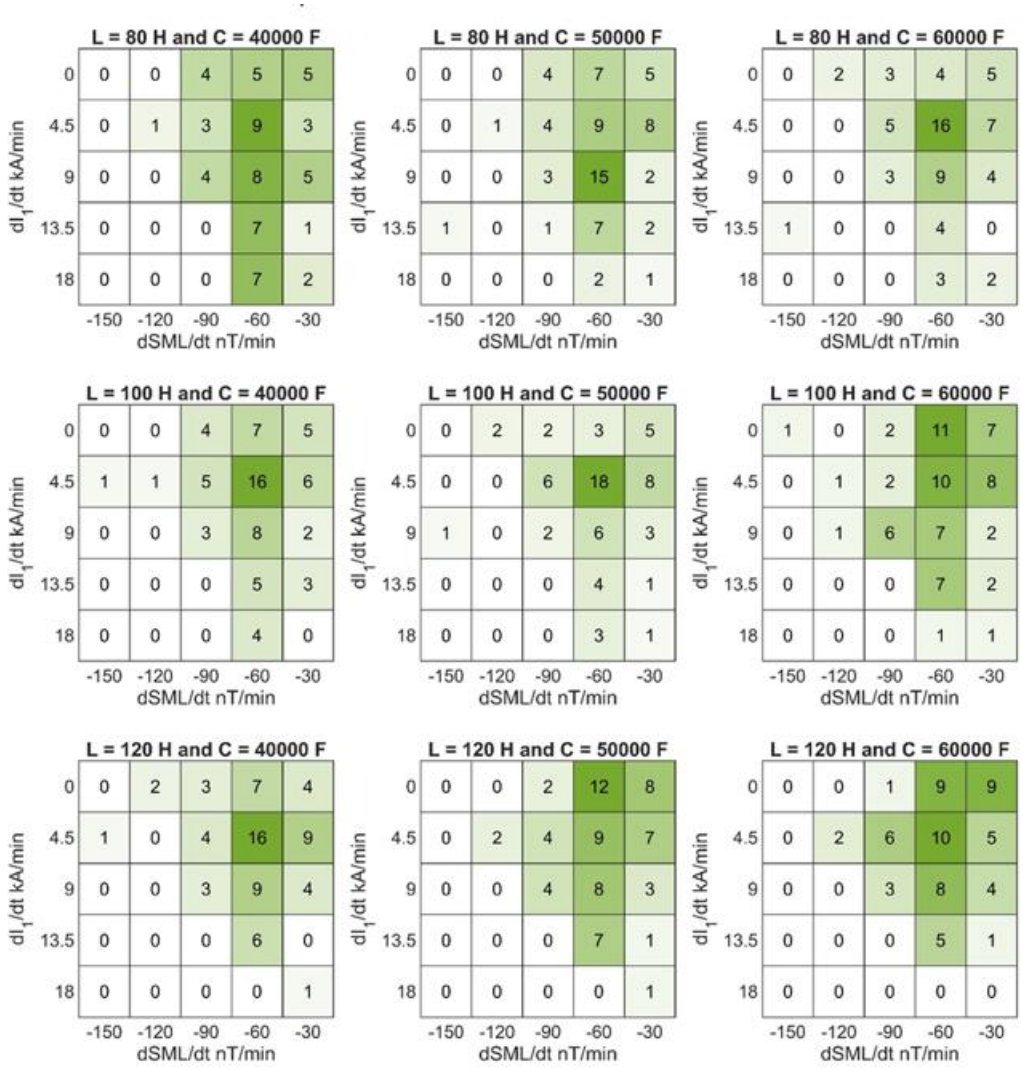

Figure 25. Plots showing the impact of 20% deviations in L and C values on dI1/dt and dSML/dt.

Building upon the analysis in Figure 24, this figure investigates the impact of 20% deviations in L and C values on dI1/dt and dSML/dt. This analysis gives more insight into how the parameters influence the model output and its dependence on time change.

The heatmaps demonstrate how substorm onset clustering tendencies change as inductance L and Capacitance C values deviate more significantly from their nominal values.

CHAPTER VI

CONCLUSION

The relationship between current and the rate of change of current (di/dt) is fundamental in the study of substorm phenomena because the slope is synonymous with dSML/dt which measures the rate of change of geomagnetic disturbances. This indicates how quickly the magnetic field changes in response to external influences. Positive current (I1) values indicate an increase in geomagnetic activity and negative indicates an equivalent decrease.

The negative current values are not essential to this research and as such are clipped off. As established, the output current depends on model parameter variations. The relationship between field-aligned current (I), and its slope, and how the relationship changes with changes in L and C values are established and shown using a heat map. The conclusions of this study are.

1. The model exhibits robustness when tau values are low, and when L and C are varied by +-5% indicating low dynamics in the system.
2. Under nominal conditions, during substorms, I1 typically falls within the range of 300-600 kA, while dI1/dt falls within the range of 6-9 kA/min.

3. The data suggests that the majority of substorms occur when SML falls between -60 to -90nT, which aligns well with the I1 values predicted by the WINDMI model, falling within the 6-9 kA/min range.
4. There will be intersections of onset times irrespective of different criteria if the magnitude of SML at onset falls between -60nT and -90nT

REFERENCES

Akasofu, S. I. (2004). Several “controversial” issues on substorms. In *Space Science Reviews* (Vol. 113, Issues 1–2). https://doi.org/10.1023/B:SPAC.0000042938.57710.fb

Bittencourt, J. A. (2004). Fundamentals of Plasma Physics. In *Fundamentals of Plasma Physics*. https://doi.org/10.1007/978-1-4757-4030-1

DeForest, S. E., & McIlwain, C. E. (1971). Plasma clouds in the magnetosphere. *Journal of Geophysical Research*, *76*(16). https://doi.org/10.1029/ja076i016p03587

Ebihara, Y., Tanaka, T., & Kamiyoshikawa, N. (2019). New Diagnosis for Energy Flow From Solar Wind to Ionosphere During Substorm: Global MHD Simulation. *Journal of Geophysical Research: Space Physics*, *124*(1). https://doi.org/10.1029/2018JA026177

Forsyth, C., Rae, I. J., Coxon, J. C., Freeman, M. P., Jackman, C. M., Gjerloev, J., & Fazakerley, A. N. (2015). A new technique for determining Substorm Onsets and Phases from Indices of the Electrojet (SOPHIE). *Journal of Geophysical Research: Space Physics*, *120*(12). https://doi.org/10.1002/2015JA021343

Frey, H. U., Mende, S. B., Angelopoulos, V., & Donovan, E. F. (2004). Substorm onset observations by IMAGE-FUV. *Journal of Geophysical Research: Space Physics*, *109*(A10). https://doi.org/10.1029/2004JA010607

Fu, H., Yue, C., Zong, Q. G., Zhou, X. Z., & Fu, S. (2021). Statistical Characteristics of Substorms With Different Intensity. *Journal of Geophysical Research: Space Physics*, *126*(8). https://doi.org/10.1029/2021JA029318

Horton, W., Pekker, M., & Doxas, I. (1998). Magnetic energy storage and the nightside magnetosphere-ionosphere coupling. *Geophysical Research Letters*, *25*(21). https://doi.org/10.1029/1998GL900043

Juusola, L., Østgaard, N., Tanskanen, E., Partamies, N., & Snekvik, K. (2011). Earthward plasma sheet flows during substorm phases. *Journal of Geophysical Research: Space Physics*, *116*(10). https://doi.org/10.1029/2011JA016852

Kamide, Y., & Akasofu, S.-I. (1975). The auroral electrojet and global auroral features. *Journal of Geophysical Research*, *80*(25). https://doi.org/10.1029/ja080i025p03585

Liu, W. W., Liang, J., Spanswick, E., & Donovan, E. F. (2007). Remote-sensing magnetospheric dynamics with riometers: Observation and theory. *Journal of Geophysical Research: Space Physics*, *112*(A5). https://doi.org/10.1029/2006ja012115

Lyon, J. G., Fedder, J. A., & Mobarry, C. M. (2004). The Lyon-Fedder-Mobarry (LFM) global MHD magnetospheric simulation code. *Journal of Atmospheric and Solar-Terrestrial Physics*, *66*(15-16 SPEC. ISS.). https://doi.org/10.1016/j.jastp.2004.03.020

Maimaiti, M., Kunduri, B., Ruohoniemi, J. M., Baker, J. B. H., & House, L. L. (2019). A Deep Learning-Based Approach to Forecast the Onset of Magnetic Substorms. *Space Weather*, *17*(11). https://doi.org/10.1029/2019SW002251

Mozer, F. S., & Pritchett, P. L. (2010). Spatial, temporal, and amplitude characteristics of parallel electric fields associated with subsolar magnetic field reconnection. *Journal of Geophysical Research: Space Physics*, *115*(A4). https://doi.org/10.1029/2009JA014718

Newell, P. T., & Gjerloev, J. W. (2011). Evaluation of SuperMAG auroral electrojet indices as indicators of substorms and auroral power. *Journal of Geophysical Research: Space Physics*, *116*(12). https://doi.org/10.1029/2011JA016779

Newell, P. T., Lee, A. R., Liou, K., Ohtani, S. I., Sotirelis, T., & Wing, S. (2010). Substorm cycle dependence of various types of aurora. *Journal of Geophysical Research: Space Physics*, *115*(9). https://doi.org/10.1029/2010JA015331

Nishimura, Y., Yang, J., Pritchett, P. L., Coroniti, F. V., Donovan, E. F., Lyons, L. R., Wolf, R. A., Angelopoulos, V., & Mende, S. B. (2016). Statistical properties of substorm auroral onset beads/rays. *Journal of Geophysical Research: Space Physics*, *121*(9). https://doi.org/10.1002/2016JA022801

Ohtani, S., & Gjerloev, J. W. (2020). Is the Substorm Current Wedge an Ensemble of Wedgelets?: Revisit to Midlatitude Positive Bays. *Journal of Geophysical Research: Space Physics*, *125*(9). https://doi.org/10.1029/2020JA027902

Partamies, N., Juusola, L., Tanskanen, E., & Kauristie, K. (2013). Statistical properties of substorms during different storm and solar cycle phases. *Annales Geophysicae*, *31*(2). https://doi.org/10.5194/angeo-31-349-2013

Partamies, N., Juusola, L., Tanskanen, E., Kauristie, K., Weygand, J. M., & Ogawa, Y. (2011). Substorms during different storm phases. *Annales Geophysicae*, *29*(11). https://doi.org/10.5194/angeo-29-2031-2011

Smith, J. P., Thiffeault, J. L., & Horton, W. (2000). Dynamical range of the WINDMI model: An exploration of possible magnetospheric plasma states. *Journal of Geophysical Research: Space Physics*, *105*(A6). https://doi.org/10.1029/1999ja000218

Spencer, E., Horton, W., Mays, M. L., Doxas, I., & Kozyra, J. (2007). Analysis of the 3-7 October 2000 and 15-24 April 2002 geomagnetic storms with an optimized nonlinear dynamical model. *Journal of Geophysical Research: Space Physics*, *112*(4). https://doi.org/10.1029/2006JA012019

Spencer, E., Rao, A., Horton, W., & Mays, M. L. (2009). Evaluation of solar wind-magnetosphere coupling functions during geomagnetic storms with the WINDMI model. *Journal of Geophysical Research: Space Physics*, *114*(2). https://doi.org/10.1029/2008JA013530

Supermag Indices. (n.d.). Retrieved November 18, 2023, from https://supermag.jhuapl.edu/indices

Tsurutani, B. T., Lakhina, G. S., & Hajra, R. (2023). Comments on "New Insights From the 2003 Halloween Storm Into the Colaba 1600 nT Magnetic Depression During the 1859 Carrington Storm" by S. Ohtani (2022). In *Journal of Geophysical Research: Space Physics* (Vol. 128, Issue 6). https://doi.org/10.1029/2022JA031034

Werner, R., Guineva, V., Despirak, I. V., Lubchich, A. A., Setsko, P. V., Atanassov, A., Bojilova, R., Raykova, L., & Valev, D. (2023). Statistical Studies of Auroral Activity and Perturbations of the Geomagnetic Field at Middle Latitudes. *Geomagnetism and Aeronomy*, *63*(4). https://doi.org/10.1134/S0016793223600303

Zhang, B., Sorathia, K. A., Lyon, J. G., Merkin, V. G., Garretson, J. S., & Wiltberger, M. (2019). GAMERA: A Three-dimensional Finite-volume MHD Solver for Non-orthogonal Curvilinear Geometries. *The Astrophysical Journal Supplement Series*, *244*(1). https://doi.org/10.3847/1538-4365/ab3a4c

BIOGRAPHICAL SKETCH

Name of Author. Mayowa Michael Kayode-Adeoye

Graduate and Undergraduate Schools Attended.
The University of South Alabama, Mobile, Alabama, USA.
University of Lagos, Akoka, Lagos, Nigeria

Degrees Awarded.
Bachelor of Science in Computer Engineering, 2018.
University of Lagos, Akoka, Lagos, Nigeria.
Master of Science in Electrical and Computer Engineering, 2023.
University of South Alabama, Mobile, Alabama, USA.

Awards and Honors.
Graduate Research Assistant 2022-2023
IEEE – HKN Honor Society
ECE Grad Student Excellence General Endowed Scholarship, 2023, University of South Alabama.